Title
Thin-Film Materials for the Protection of Semiconducting Photoelectrodes in Solar-Fuel Generators

Journal
The Journal of Physical Chemistry C, 119(43)

ISSN
1932-7447

Authors
Hu, Shu
Lewis, Nathan S
Ager, Joel W
et al.

Publication Date
2015-10-29

DOI
10.1021/acs.jpcc.5b05976

Peer reviewed

THE JOURNAL OF PHYSICAL CHEMISTRY C

Review Article

pubs.acs.org/JPCC

Thin-Film Materials for the Protection of Semiconducting Photoelectrodes in Solar-Fuel Generators

Shu Hu,[†,‡] Nathan S. Lewis,[*,†,‡,§,∥] Joel W. Ager,[⊥,#] Jinhui Yang,[⊥,#] James R. McKone,[¶] and Nicholas C. Strandwitz[*,□]

[†]Division of Chemistry and Chemical Engineering, [‡]Joint Center for Artificial Photosynthesis, [§]Beckman Institute, and [∥]Kavli Nanoscience Institute, California Institute of Technology, Pasadena, California 91125, United States

[⊥]Joint Center for Artificial Photosynthesis and [#]Materials Sciences Division, Lawrence Berkeley National Laboratory, Berkeley, California 94720, United States

[¶]Department of Chemistry and Chemical Biology, Cornell University, Ithaca, New York 14853, United States

[□]Department of Materials Science and Engineering and Center for Advanced Materials and Nanotechnology, Lehigh University, Bethlehem, Pennsylvania 18015, United States

ABSTRACT: The electrochemical instability of semiconductors in aqueous electrolytes has impeded the development of robust sunlight-driven water-splitting systems. We review the use of protective thin films to improve the electrochemical stability of otherwise unstable semiconductor photoelectrodes (e.g., Si and GaAs). We first discuss the origins of instability and various strategies for achieving stable and functional photoelectrosynthetic interfaces. We then focus specifically on the use of thin protective films on photoanodes and photocathodes for photosynthetic reactions that include oxygen evolution, halide oxidation, and hydrogen evolution. Finally, we provide an outlook for the future development of thin-layer protection strategies to enable semiconductor-based solar-driven fuel production.

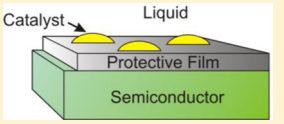

1. INTRODUCTION

Photoelectrochemical (PEC) systems capture the energy of sunlight and enable the storage of that energy in the chemical bonds of a commodity chemical or fuel, such as hydrogen. Chemical fuel can be used to power vehicles or to generate electricity on demand, in contrast to photovoltaic systems that cannot generate electricity during cloudy weather or at night. Efficient, inexpensive, and long-lasting PEC systems that could allow for the harvesting and storage of a small fraction (0.02%) of the ∼96 000 TW of solar power incident on the surface of the earth could, in principle, meet all current global fuel and electricity needs.[1]

In general, a PEC system uses light-absorbing materials, such as semiconductors or molecular systems, to capture photons and convert the energy of the photons to excited states of charge carriers. The internal energy in these excited states can be transported to the interface between the light absorber and an electrolyte, at which reactive sites can facilitate oxidative or reductive electron-transfer half-reactions. The reductive half-reaction produces a chemical fuel, whereas the oxidative half-reaction produces O_2 or another chemical oxidant, such as halogens: I_2, Br_2, or Cl_2. Because electrolysis of halide compounds also stores energy in the form of renewable H_2 fuel, hydrogen halide splitting is also technologically relevant to solar-fuel production. Protons or hydroxide ions liberated by one-half-reaction must be transported to the sites where the other half-reaction occurs. The products of the overall reaction, a chemical fuel and an oxidant, may be formed and collected in a single compartment, yielding a system that produces a mixture of reactive products that subsequently must be separated. Alternatively, the oxidation and reduction reactions can be carried out in separate compartments; this configuration obviates the need for a subsequent separation strategy but often impedes the requisite mass transport to neutralize chemical potential gradients while minimizing product crossover.

Solar-driven water-splitting cells that specifically use semiconducting materials to produce $H_2(g)$ and $O_2(g)$ from water have been a focus of much recent research attention, as evidenced by the extensive recent review literature and commentary.[2−11] In context of the preceding paragraph, semiconductors are responsible for light absorption, and photocathodes and/or photoanodes drive the hydrogen-evolution reaction (HER) and oxygen-evolution reaction (OER), respectively. A single semiconductor (e.g., $SrTiO_3$) under solar illumination can generate charge carriers that have sufficient electrochemical potential difference to split water under standard conditions at room temperature. However, such materials can only absorb photons with energies in the ultraviolet (>3 eV) and thus cannot effectively convert an appreciable amount of energy available in the visible and infrared portions of the solar spectrum, leading to low terrestrial solar-to-hydrogen conversion efficiencies.[12]

One of the primary strategies for realizing an efficient water-splitting cell is to use two semiconducting light absorbers placed optically and electrically in series. In this tandem-absorber approach, the total electrochemical potential available

Received: June 22, 2015
Revised: September 25, 2015

DOI: 10.1021/acs.jpcc.5b05976
J. Phys. Chem. C XXXX, XXX, XXX−XXX

to drive the water-splitting reaction is ideally the sum of the photovoltages produced by each semiconductor. Electrochemical water splitting requires a minimum potential difference of 1.23 V between the anode and cathode under standard conditions; however, kinetic barriers to the HER and OER are overcome only when a substantial overpotential (at least 0.3–0.4 V) is applied. Thus, in addition to semiconducting light absorbers, efficient solar-driven water splitting requires electrocatalysts to minimize the required overpotential. Figure 1a,b shows a schematic for tandem-absorber-based water-splitting cells operating in acidic and alkaline aqueous solutions, respectively.

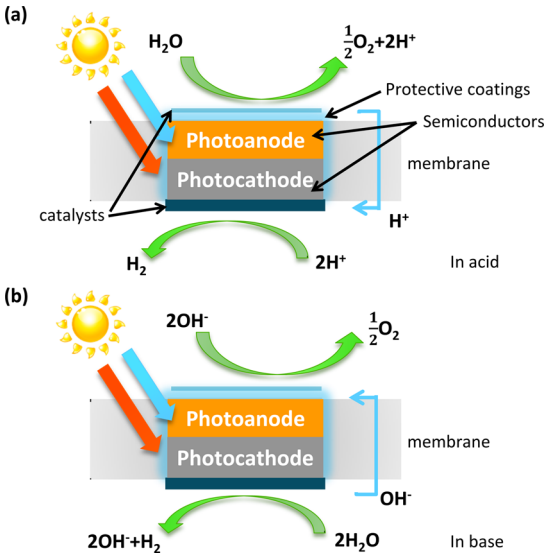

Figure 1. Schematic of a tandem-absorber-based solar-driven water-splitting cell operating in (a) acidic and (b) alkaline aqueous solution. The light absorbers are semiconductors arranged in series with respect to the direction of the incident light, with the bottom semiconductor absorbing lower-energy photons than those absorbed by the top semiconductor. The light absorbers support oxygen-evolution and hydrogen-evolution catalysts which are in physical contact with an aqueous electrolyte, and the light absorbers are embedded in a gas-impermeable ion-exchange membrane. A protective coating conformally covers and passivates the top and sides of the tandem light absorber component of the system, while allowing for integration of catalysts on the outer surface.

The requirements associated with a tandem-absorber strategy for solar-driven water-splitting cells have been analyzed in detail, and these criteria can be used to identify suitable semiconductor absorbers.[13−17] An optimized tandem-junction solar-driven water-splitting system consists of a semiconductor with a band gap of 1.60–1.80 eV on the top and a semiconductor with a band gap of 0.95–1.20 eV on the bottom, with the exact values depending on the performance of the electrocatalysts and design of the water-splitting cell.[15] These band gap requirements rule out the use of most known oxide semiconductors ($SrTiO_3$ and TiO_2, for example) and suggest the suitability of well-understood and technologically important Group IV, III–V, II–VI, and chalcopyrite semiconductors as light absorbers. However, these latter materials are typically unstable (either dissolving or developing insulating oxide coatings) under aqueous HER or OER conditions. Thus, the efficiency requirements of a viable water-splitting system present a materials conundrum: known chemically stable oxide semiconductors are unsuitable due to inappropriately large band gaps (e.g., $SrTiO_3$) and/or poor electronic properties (e.g., Fe_2O_3), while the technologically important semiconductors with appropriate band gaps (e.g., Si, GaAs) that accordingly are used in photovoltaic cells cannot be used in PEC-based systems directly due to the chemical instability of the photoelectrode materials. Two parallel paths are being pursued in response to this conundrum: (1) develop methods to protect those otherwise unstable semiconductors to enable their use in efficient water-splitting cells and (2) discover new, efficient semiconductors that are inherently stable under water-splitting conditions and that have band gaps in the range of 0.95–1.8 eV.

In developing PEC materials along either path described above, one must consider the environment in which the electrochemical reactions are carried out. An efficient water-splitting cell must make use of electrolytes that can support sizable photocurrent densities, typically ≥10 mA cm^{-2} under nonconcentrated "1 Sun" illumination. In the absence of external energy inputs other than sunlight, operation at this current density corresponds to ≥12.3% solar-to-hydrogen conversion efficiency.[18] Inefficient ion transport will result in the development of a significant potential gradient in the cell, which will be manifested in part as a pH gradient in the aqueous electrolytes as well as possible concentration gradients associated with the transport of other ionic species in the electrolyte. Strongly acidic or alkaline electrolytes (pH < 1 or pH > 13, respectively) are capable of supporting the requisite current densities without developing significant pH gradients.[19] However, many semiconductors are chemically unstable in contact with such potentially corrosive electrolytes. Thus, the discovery of electrocatalysts, semiconductors, and protective barriers that are stable in highly acidic or alkaline media is one of several key hurdles to realize a technologically viable, efficient, safe, and stable tandem solar-driven water-splitting system.[20,21]

Several reviews have recently been published that describe aspects of semiconductor-based solar-driven water splitting. These include a general review of water-splitting cells,[2] experimental demonstrations,[11] Si-based materials,[22] and surface passivation layers with a focus on the electronic properties of the resulting devices.[23] This review focuses on the use of thin-film materials to protect and stabilize otherwise unstable semiconductors for use as photoelectrodes in water-splitting systems. First, we discuss the origins of the chemical instability of materials and semiconductors specifically (Section 2). Additional background in Section 2 includes a discussion of strategies for realizing stable semiconductor/liquid junctions, which identifies thin protective films as a promising strategy. We then discuss various techniques for the formation of such coatings and how they impact interfacial electronic behavior. The literature that describes thin films for use as protective layers for photoanodes (Section 3) and photocathodes (Section 4) using unstable semiconducting light absorbers in water-splitting devices is then thoroughly reviewed. Finally, we present an outlook for the future of protective thin films to enable the robust, efficient production of solar fuels under a variety of operational conditions (Section 5).

2. BACKGROUND ON INSTABILITY AND STABILIZATION STRATEGIES

Corrosion of semiconductor electrodes represents a special case of the general phenomenon and conceptual treatment of

DOI: 10.1021/acs.jpcc.5b05976
J. Phys. Chem. C XXXX, XXX, XXX–XXX

corrosion of electroactive substances, including metals, oxides, and other conductive materials. According to Pourbaix, corrosion is "the destruction of a material under the chemical or electrochemical action of the surrounding environment".[24] In the context of this broad definition, corrosion poses a ubiquitous practical challenge for long-term materials stability. Corrosion processes have been most thoroughly characterized for metals in aqueous environments, for which corrosion generally occurs through the oxidation of zerovalent species, as in eq 1.

$$M + ox \rightarrow M^{z+} + red \quad (1)$$

Here, M is a zerovalent metal; M^{z+} is the oxidized metal product; ox is an oxidant; and red is the reduced form of the oxidant. The reduction process accompanying metal oxidation usually involves the conversion of protons to H_2 or reduction of oxygen to water. Both of these processes involve Brønsted–Lowry acid equivalents, so the pH of the electrolyte is a critical parameter in determining the thermodynamics of corrosion of metals.

Sustained rapid corrosion requires that the relevant reaction is thermodynamically favorable as well as kinetically facile. However, even extremely slow corrosion can have a significant impact on the lifetime of industrial components (e.g., turbine blades, vehicle chassis, etc.), so thermodynamic calculations are generally considered to be the most important indicator of long-term material stability. For example, Pourbaix diagrams, or potential-pH predominance area diagrams, provide useful relationships between the stable phase and the electrochemical potential of the solid and solution environment.[25] Figure 2 shows, by way of example, the potential-pH diagram for titanium.

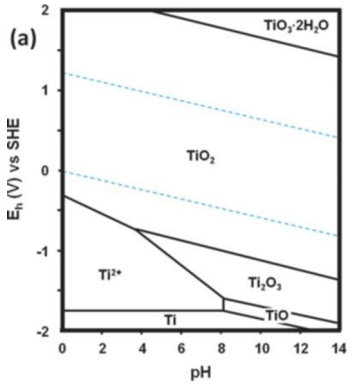

Figure 2. Pourbaix diagram for titanium in aqueous electrolytes, adapted from ref 25. Both H_2 evolution and water oxidation occur in the passivating region of the diagram. Reproduced by permission of The Electrochemical Society.

Several strategies for corrosion protection in aqueous environments have been implemented. The most straightforward approach involves use of a chemically stable coating. For example, Ti has a large passivation region involving the formation of a surface oxide layer, with this passivation region covering practical potential-pH values for both water oxidation and H_2 generation (Figure 2). Indeed, in pH 0–14 electrolytes, bulk titanium dioxide (TiO_2) is chemically stable at up to 600 mV anodic overpotentials and 200 mV cathodic overpotentials with respect to the OER and HER, respectively.

Many surface coatings that are used to prevent corrosion in metals are not suitable for use in semiconductor-based water splitting systems. First, thick metallic or insulating films are not universally applicable to semiconductor photoelectrodes because such films block light from reaching the semiconductor and/or impede the charge transfer processes that are required to effect the fuel-forming interfacial redox reactions that must be sustained in an operating water-splitting cell. Another method that is commonly used to protect metals from corrosion involves electrically connecting the material to be protected to a sacrificial anode that is more favorably oxidized. The connection causes the electrochemical potential of the metal to rest in the passivation or immunity region on a potential-pH diagram.[27] In an analogous fashion, applied potentials can be used to protect metals from corrosion. This approach only works for PEC systems if a region of electrochemical potential stability happens to coincide with the potentials needed for the fuel-forming redox reactions. Such a situation is more likely to occur for photocathodes than photoanodes and, as such, will be discussed further in Section 4.

Corrosion of semiconductors is more complicated than corrosion of metals because the number of available electrons or holes at the surface that participate in electrochemical processes varies depending on the illumination, biasing conditions, surface/bulk electronic properties, and the solution composition. Further, many semiconductor materials of interest contain several different atoms, which allows for multiple corrosion mechanisms, each governed by different electrochemical equilibria.

The corrosion of semiconductor photoelectrodes can occur through three routes: photoelectrochemical, electrochemical, and chemical. Electrochemical and photoelectrochemical corrosion both require net charge transfer between the photoelectrode and the electrolyte; however, photoelectrochemical reactions involve photoexcited minority carriers, whereas electrochemical reactions involve majority carriers. Chemical corrosion involves reactions that lead to degradation or dissolution of the electrode material without the necessity of net charge transfer across the solid–electrolyte interface.

In the 1970s, Gerischer recognized the issue of photoelectrochemical corrosion of inorganic semiconductors and conducted an analysis of the corrosion potentials of several compound semiconductors.[28] In particular, Gerischer related the quasi-Fermi levels of the minority carriers to the corrosion potential to determine if a given corrosion reaction was thermodynamically favorable when the semiconductor was illuminated. Figure 3 shows the band gap–corrosion potential relationships for stable and unstable semiconductors, using the band diagram formalism. The aqueous photocorrosion reactions for anodic and cathodic decomposition of a covalent compound semiconductor, respectively, can be written as

$$MX + zh^+ \rightarrow M^{z+}{}_{(aq)} + X \quad (2)$$

$$MX + ze^- \rightarrow M + X^{z-}{}_{(aq)} \quad (3)$$

where M and X are the semiconductor cation and anion; zh^+ is the stoichiometric number of holes; and ze^- is that of electrons. The same reactions can proceed for an elemental semiconductor (e.g., Si), where formally M and X are the same zerovalent element.

As implied by eqs 2 and 3, the oxidized component (M) may become solvated by the aqueous solution through coordination with water or adventitious components of the electrolyte.

DOI: 10.1021/acs.jpcc.5b05976
J. Phys. Chem. C XXXX, XXX, XXX–XXX

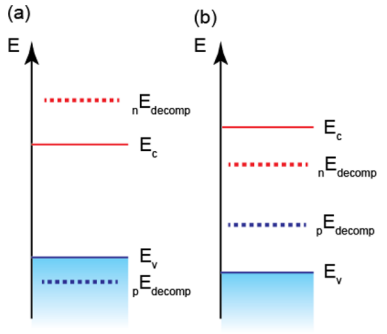

Figure 3. (a) Stable and (b) unstable band alignment for semiconductor electrodes where $_nE_{decomp}$ indicates the cathodic decomposition potential and $_pE_{decomp}$ indicates the anodic decomposition potential.

Alternatively, corrosion can produce insoluble species, which often remain attached to the surface of the semiconductor as a thin film and retard further corrosion. Regardless of the details of each given corrosion reaction, the position of the quasi-Fermi level with respect to the corrosion potential determines whether the photocorrosion process is thermodynamically favorable under illumination.

The studies by Gerischer were followed by further analysis of semiconductor stability by Park and Barber[29] and by Fujishima et al.[30] More recently, these analyses have been augmented with modern thermodynamic data and first-principles calculations, to provide a more general analysis for a wide range of semiconductors.[31] Results to date indicate that all known nonoxide semiconductors are unstable during aqueous anodic oxygen evolution, and only a few materials, such as Si and WSe_2, are stable under cathodic conditions.[32]

Although in many cases the corrosion of a semiconducting light absorber is driven by optical excitation, the corrosion reaction can also occur over a wide range of potentials in the dark. For example, dissolution of Si in alkaline media cannot be completely inhibited by varying the electrode potential. Attempts to quantify the contributions of the electrochemical corrosion and chemical corrosion processes indicate that chemical rather than electrochemical mechanisms dominate the dissolution of Si in alkaline media.[33,34] Therefore, the changes in surface electron/hole concentrations due to optical excitation and/or biasing can change the electrochemical corrosion rates, but such treatments may not completely arrest the corrosion of Si.

Several general conclusions can be drawn from the above discussion. First, corrosion is ubiquitous for nonoxide semiconductors that have suitable band gaps for tandem-based PEC water electrolysis. Second, such corrosion can give rise to two outcomes: passivation and dissolution. Passivation involves corrosion reactions that result in a protective and insoluble film. For example, anodization of Si in neutral solutions produces a surface layer of SiO_2, which is insoluble in many acidic and neutral electrolytes. Alternatively, dissolution involves a change in redox state and removal of dissolved semiconductor atoms from the surface, such as the oxidation of Si and dissolution as silicate species in strongly alkaline solution.

In many cases of passivation, including Si oxidation, the passivating film is not electrically conductive, rendering this region locally inactive for electrochemical reactions, but possibly protected from further corrosion. As a result, passivation can be used as a viable strategy for protection of semiconductor photoelectrodes in specific cases. Dissolution is arguably less desirable than passivation because dissolution results in the continual destruction of the semiconductor and can undercut protected regions, thus ultimately leading to failure that propagates throughout entire active regions. Only semiconductors whose dissolution rates are *extremely* kinetically inhibited can achieve sustained PEC-based solar-driven water splitting without additional surface protective treatments.

2.1. Strategies for Obtaining Stable Semiconductor/Liquid Junctions. Given the ubiquity of semiconductor corrosion, several strategies for stabilizing semiconductor/liquid junctions have been developed to mitigate this drawback. We discuss all of the strategies here for context and subsequently describe in detail the specific approach of surface coatings, which has proven to be the most successful for applications of semiconductor photoelectrodes for solar-driven water splitting.

One strategy for making stable semiconductor/liquid junctions involves the scrupulous removal of water and oxygen from the system, thus removing the reactants for the most common corrosion reactions. Nonaqueous redox systems (e.g., ferrocene dissolved in acetonitrile containing a supporting electrolyte) can yield stable PEC systems[35−37] and can also provide a simple, corrosion-free platform for evaluating the electronic properties of semiconductor absorbers. These systems can be used to produce regenerative PEC cells that produce electricity but do not store energy as chemical fuels and cannot be used directly for water splitting. Regenerative aqueous systems can also exhibit long-term stability by exploiting electrolytes that facilitate kinetic stabilization.[38−42] In such cases, the desirable interfacial electron-transfer reaction kinetically outcompetes the oxidation or reduction of the semiconductor photoelectrode, resulting in greatly suppressed rates of corrosion. Although kinetic stabilization is possible in the regenerative PEC case, for which the oxidation/reduction of the solution redox pair is extremely rapid, oxygen evolution and hydrogen evolution are generally slower than the corrosion reactions and hence lead to high branching ratios of electrochemical corrosion relative to the desired water-splitting chemistry. Exceptions to this general rule likely exist for oxide semiconductors. For example, kinetic stabilization may explain the increased robustness of Fe hydroxide- or CoO_x-functionalized $BiVO_4$, where the corrosion/photopassivation of this oxide semiconductor is slower than water oxidation by Fe hydroxide or CoO_x.[43,44]

Surface functionalization by organic reagents has been explored for stabilization and manipulation of the interfacial energetics and kinetics of semiconductor electrodes in aqueous electrolytes. Functionalization of surfaces with covalently bonded organic moieties can enhance the stability of semiconductor electrodes.[45] One of the most studied systems in this regard is the methyl-terminated Si(111) surface because nearly 100% of the surface Si atop sites can be functionalized with a methyl group.[46] While such molecular functionalization may provide stable photocathodes due to the lack of a reductive degradation mechanism, such functionalization for photoanode stabilization is likely to be limited in general because aliphatic C−H bonds are more readily oxidized than water or hydroxide ions. As an example of utility for photocathodes, p-Si has been functionalized with a modified viologen that acts as a support and charge-transfer layer for Pt particles that electrocatalyze H_2 production in water.[47]

DOI: 10.1021/acs.jpcc.5b05976
J. Phys. Chem. C XXXX, XXX, XXX−XXX

The primary approach, and the focus of this review, is the strategy of coating unstable semiconductor surfaces with thermodynamically stable films (Figure 4).[48] In this case, the

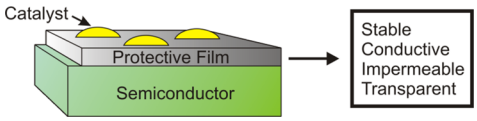

Figure 4. Schematic of a protective film for photoelectrochemical fuel generation depicting only the semiconductor near-surface region, the protective film, catalysts, and the solution, along with the properties required of the film.

protective film should be electrically conductive, electrochemically stable, and optically transparent and should prevent the semiconductor surface from directly contacting the electrolyte. Ideally, such a layer would also possess favorable optical and electronic properties (e.g., highly transparent and perhaps antireflective; large barrier for transfer of majority carriers; small interface trap state density). Clearly, not all coatings will fulfill all of these requirements. For example, thick (i.e., more than a few nanometers) metal films will not be antireflective or optically transparent and will generally produce low open-circuit voltages when relied upon for the formation of the photoactive junction (i.e., Schottky contact), so the utility of such films is likely limited. In some cases, the protective film could be catalytic for the reaction of interest; however, catalysts or cocatalysts can also be added to the outer surface or incorporated as an additional component in the protective layer. The composition of the protective film, the deposition technique, and the structure at the interface can play significant roles in determining the resulting photoelectrosynthetic behavior.

The location and coverage of conductive and protective films are also relevant parameters that must be considered. Variation of such geometric factors includes the patterning of 2D metal islands[49] where the metal protective contacts can be optically thick, provided that the islands are sparse enough to allow for passage of a large fraction of solar light. Further, strategies including 3D structuring, and the passage of current through optically thick metal films[50] or metal particles at the base of high aspect ratio structured absorbers, have been proposed[10,21] and implemented experimentally.[51,52] While these strategies may enable the use of optically thick catalytic/protective films in well-defined locations, protection is still required on the remainder of the semiconductor surface where the requirement of electronic conductivity is lifted, but transparency and stability are not.

2.2. Methods for Forming Protective Films. Various techniques can be employed for forming protective films on semiconductor light absorbers, each with its own basic principles and merits. Broadly, the deposition technique chosen will influence the uniformity, stoichiometry, interfacial characteristics, and other structural and electronic properties of the film and hence may critically impact the stability and performance of the resulting composite photoelectrodes.

Physical-vapor deposition (PVD) techniques, such as thermal or electron-beam evaporation, magnetron sputtering, and pulsed-laser deposition, allow for precise control over the composition and thickness of the protective film. The principle drawback of PVD techniques is line-of-sight deposition, which can result in shadowing and inhomogeneous deposition on structured semiconductor surfaces. This drawback can be somewhat circumvented by tuning the deposition conditions (e.g., chamber pressure and deposition geometry). Sputtering is one of the most common and popular PVD methods, but it can result in damage to the semiconductor absorber surface due to impact of high-energy ions.[53] Another drawback of PVD techniques broadly is the lack of chemical control at the interface between the semiconductor and the deposited film.

Chemical vapor deposition (CVD) techniques have also been used for forming corrosion protection coatings. These techniques are limited by the precursor volatility, stability, and deposition chemistry, all of which limit the available deposition conditions and material compositions. CVD can be used to coat nonplanar surfaces under appropriate deposition conditions. Atomic-layer deposition (ALD), the subset of CVD techniques that utilizes sequential, self-limiting surface reactions, is particularly suitable for conformal and uniform deposition on high aspect-ratio or porous materials.[54] Further, ALD exhibits a high degree of thickness control relative to traditional CVD and PVD techniques. Due to these advantages, a large number of recent studies on the protection of photoelectrodes have used ALD.

Electrodeposition is another well-studied technique that can coat high aspect-ratio materials and generally deposits material where a conductive path and precursor species are simultaneously present. This technique is limited by the deposition conditions (e.g., near room temperature, liquid environment) and generally results in porous coatings.[55] A heavily investigated method of catalyst formation is the electrodeposition of Co and Ni oxides,[56] which result in a porous film that maximizes the number of sites for catalysis. However, the resulting film is unsuitable for corrosion protection of nonoxide semiconductors due to porosity. Sol–gel, chemical bath, and spray deposition of materials are also of interest due to their low cost of implementation, but like electrodeposition, these techniques often result in porous films that can even remain somewhat porous after postdeposition annealing/densification steps.[57,58]

2.3. Behavior of Semiconductor/Electrolyte Interfaces. The deposition chemistry, as well as the structure of the resulting semiconductor/protective film interface, can significantly influence the resulting electronic properties and hence the energy-conversion efficiency of photoelectrodes. Figure 5

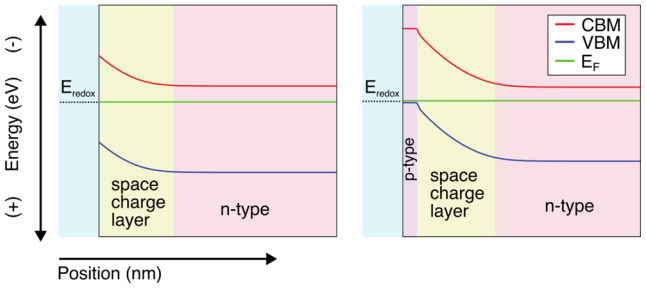

Figure 5. Comparison of energy band diagrams for a semiconductor/liquid PEC junction (left) and for a buried PV junction (right). The base semiconductors in both cases are doped n-type. In the buried PV junction case, a p-type thin layer or a semiconductor/metal Schottky barrier forms a different, and often higher, built-in voltage than the contact with the electrolyte, depending on the value of E_{redox} and the interfacial energetic situation of the different types of contacts on the semiconductor of interest.

DOI: 10.1021/acs.jpcc.5b05976
J. Phys. Chem. C XXXX, XXX, XXX−XXX

shows two contrasting cases, specifically photovoltaic (PV) cells that utilize "buried", solid-state junctions, as well as photoelectrochemical (PEC) cells using semiconductor−liquid junctions. The terminology used here in differentiating between PV and PEC junctions was recently clarified in a report on the taxonomy of solar fuel generators.[10] For PEC cells, the band bending responsible for charge separation is produced by charge-transfer equilibration between the Fermi level of the semiconductor and the Fermi level (electrochemical potential) of the liquid contact. In contrast, for buried-junction PV cells, the band bending in the semiconductor is entirely determined by the nature of the solid-state contact (e.g., p−n junction or semiconductor/metal junction).[59,60]

A prototypical buried junction is insensitive to changes in the redox potential of the electrolyte because the built-in voltage of the junction is determined by the solid/solid interface, not by charge transfer at the solid/liquid interface. The introduction of protective layers often converts a PEC cell into a PV cell or into a hybrid junction that incorporates aspects of a semiconductor/liquid junction as well as aspects of a solid-state junction.[61,62] Many attempts to stabilize PEC materials have used the photovoltaic junction configuration because the energy-conversion properties of such systems are essentially fixed and can often provide near optimal values of key photovoltaic figures of merit, such as the open-circuit photovoltage, V_{oc}. Consistent with the majority of recent research efforts in this area, this review focuses only on PEC cells, PV cells, and combinations of these that are fully immersed in aqueous solution. PV-biased electrosynthetic cells that involve the complete structural encapsulation of complex PV components, connected to a discrete and stand-alone electrolysis unit, while also interesting and in many ways more technologically mature, are outside the scope of this review.

For the specific absorber materials of concern, the photoelectrode performance can be estimated based on the specific junction configurations. That is, semiconductor−liquid photoelectrochemical junctions and solid-state junctions often produce different figures of merit, most notably exhibiting different open-circuit voltages (V_{oc}) under an otherwise mutually common set of conditions. For example, Si p−n junctions typically exhibit (V_{oc}) of 0.55 V or more and photocurrent densities of ≥35 mA·cm^{-2} under 1 Sun illumination.[63] For a Si Schottky barrier (direct MS contact), the V_{oc} would only be ∼0.3 V for n-type Si and ∼0.2−0.3 V for p-type Si[64,65] but could be up to 0.65 V for a MIS (metal−insulator−semiconductor) structure.[66] In all cases, direct metal−silicon contacts will result in high thermionic emission currents and thus exhibit inherently low V_{oc} values compared with well-produced p−n junctions or heterojunctions. Therefore, it is instructive to note the specific junction types employed in the work discussed below when comparing the performance of different types of coatings on a photoelectrode material of interest.

3. PROTECTION OF PHOTOANODES

3.1. Overview. Due to the early observation of photocorrosion in aqueous electrolytes, in conjunction with the general instability of nonoxide photoanode materials, significant attention has been devoted to protection of photoanodes.[28,31] This section focuses on thin-layer materials that stabilize semiconductor light absorbers for the sunlight-driven oxidation of water or hydroxide, as well as for anode reactions that are important processes in photosynthetic halide-splitting reactions. Hence, the key oxidative electrochemical half-reactions are

$$H_2O \leftrightarrow \frac{1}{2}O_2 + 2H^+(aq) + 2e^-$$

$$E^0 = 1.23\ \text{V vs RHE (in acid)}$$

$$2OH^-(aq) \leftrightarrow \frac{1}{2}O_2 + H_2O + 2e^-$$

$$E^0 = 1.23\ \text{V vs RHE (in base)}$$

$$Cl_2(g) + 2e^- \leftrightarrow 2Cl^-(aq) \quad E^0 = 1.39\ \text{V vs RHE (in acid)}$$

$$Br_2(aq) + 2e^- \leftrightarrow 2Br^-(aq)$$

$$E^0 = 1.09\ \text{V vs RHE (in acid)}$$

$$I_3^-(aq) + 2e^- \leftrightarrow 3I^-(aq) \quad E^0 = 0.54\ \text{V vs RHE (in acid)}$$

where RHE is the potential of the reversible hydrogen electrode.

Below, we present data compiled from a large number of reports of oxygen-evolving photoanodes that have been stabilized with thin films. We summarize the available library of metal oxides for protective coatings because metal oxides are generally considered thermodynamically stable for oxidative chemistry and also because the corrosion behavior of metal oxides is well-documented. Coating strategies will then be discussed and are categorized by the protective thin-film composition, including metals and metal silicides, oxides, phosphides, and nitrides, as well as organic layers.

Table 1 summarizes reported efforts to produce thin-layer protection for oxygen-evolving photoanodes. In chronological order, the table lists the semiconductor being protected, the protective film composition, deposition method, and electrolyte(s) used. When possible, the stability and performance metrics are also noted, including the time during which a noted current density was passed, the approximate onset potential vs the reported reference potential, and vs the Nernst potential for the oxidation reaction of interest. If not specified specifically in the work, the approximate onset potential was estimated as the potential at which the photocurrent reached ∼1 mA cm^{-2}. A value for V_{shift} is also reported, based on the absolute value of the shift along the potential axis in the current density vs potential curve (J−E) of an illuminated protective film, relative to the behavior of a photoinactive metallic electrode in the dark with the same near-surface composition (i.e., same electrocatalytic behavior).[20] This figure of merit is related to the photovoltage generated or "power saved" by the semiconductor absorber relative to the dark electrocatalysis case[18] and therefore quantifies the maximum free energy for the photosynthetic oxidation reaction that is produced by illumination of the photoanode. Table 1 does not include reports of thin-layer protection in nonphotosynthetic redox systems, although many of these reports will also be discussed.

A variety of reference electrodes have been used historically to evaluate the electrochemical behavior of stabilized oxygen-evolving photoanodes. A reversible hydrogen electrode (RHE) is often used to report potential values and provides a convenient reference potential because the value of RHE accounts for the actual composition of the electrolyte and represents a fixed potential relative to the reaction of interest (−1.23 V vs the reversible OER potential at 25 °C). Other reference electrodes that are often used include the saturated

DOI: 10.1021/acs.jpcc.5b05976
J. Phys. Chem. C XXXX, XXX, XXX−XXX

Table 1. Photoelectrosynthetic Systems for Oxygen Evolution[d]

year	base SC	coating (thickness, nm)[a]	deposition method	electrolyte	pH	stability, time (at J, mA cm^{-2})	E_{onset} vs ref (V)	E_{onset} vs OER (V)[b]	Vshift[c] (mV)	ref
1975	n-GaP	Au(–)	evaporation	borate buffered 0.5 M K_2SO_4	9.2	–	+0.5 vs SCE	+0.05	560	Nakato[70]
1975	n-GaP	Pd(–)	evaporation	borate buffered 0.5 M K_2SO_4	9.2	–	–	–	600	Nakato[70]
1977	n-GaP	Au(40)	sputter or evaporation	buffered 0.5 M K_2SO_4	4.3	–	−0.45 vs SCE	−1.18	300−500	Harris[71]
1977	n-GaP	Ag(30)	sputter or evaporation	buffered 0.5 M K_2SO_4	4.3	–	−0.5 vs SCE	−1.23	–	Harris[71]
1977	n-Si, n-GaAs, n-GaP, n-InP, n-CdS	TiO_2(–)	CVD	Na_2SO_4	–	w	–	–	–	Kohl[140]
2014	n-GaP	TiO_2(118)/ NiO_x(2)	ALD, e-beam evaporation	1 M KOH	13.7	>5 h (2.5)	−0.16 vs SCE	−0.35	590	Hu[49]
1977	n-GaAs, n-GaAlAs	Al_2O_3, TiO_2, Si_3N_4	sputtering	Na_2SO_4 + NaOH	-	–	–	–	–	Tomkiewic[141]
1977	n-GaAs, n-GaAlAs	SnO_2, Nb_2O_5	electrodep	Na_2SO_4 + NaOH	-	–	–	–	–	Tomkiewicz[141]
1987	n-GaAs	Pt or Pd(–)/MnO_x(20)	chemical bath deposition	0.5 M NaOH	13	>80 min (11)	−0.4 vs NHE	−0.86	–	Kainthla[91]
1994	n-GaAs	ITO(230)	sputtering	0.5 M $NaClO_4$	–	–	–	–	–	Kraft[79]
2014	np$^+$-GaAs	TiO_2(118)/Ni/NiO_x(2)	ALD, e-beam evaporation	1 M KOH	13.7	>25 h (14)	−0.38 vs SCE	−0.57	810	Hu[49]
1975	n-Si	Au(–)	evaporation	borate buffered 0.5 M K_2SO_4	9.2	–	–	–	170	Nakato[70]
1975	n-Si	Pd(–)	Evaporation	borate buffered 0.5 M K_2SO_4	9.2	–	–	–	150	Nakato[70]
1980	n-Si	Fe_2O_3(2.5-800)	sputtering/oxidation	0.1 M NaOH	13	–	+0.4 vs SCE	+0.2	–	Morisaki[83]
1983	n-Si	ITO(3-100)/RuO_2(–)	sputtering	buffered NaOH	12	–	+0.2 vs SCE	−0.1	–	Hodes[76]
1984	n-Si	Fe_2O_3(75)/Pd(10)	electron-beam evaporation	0.2 M KOH	13.3	–	+0.36 vs Hg/HgO	+0.01	–	Osaka[86]
1984	n-Si	Pt-SiO_x(10)/Pt	phototoanodic oxidation	0.5 M H_2SO_4	0	100 h (1)	+1.4 vs NHE	+0.17	–	Bockris[82]
1986	n-Si	Pt or Pd(–)/MnO_x(20)	chemical bath deposition	0.5 M K_2SO_4	13, 7	600 h (1)	+0.6, +1.2 vs NHE	+0.14, +0.38	500, 500	Kainthla[90]
1987	n$^+$n-Si, n+p-Si	Ni(30)	sputtering	1 M KOH	14	∼45 min	+0.25 vs Hg/HgO	−0.06	370	Guiozheng[142]
1987	n$^+$n-Si, n$^+$p-Si	Pt(3)	sputtering	1 M KOH	25	>8 h	+0.51 vs Hg/HgO	+0.2	170	Guiozheng[142]
1989	n-Si	Cr_2O_3(–) /TiO_2(–)/ SbO_x(–)	CVD/sol−gel	1 M H_2SO_4 + 1 M IPA	∼0	20 h (2.0)	+0.5 vs SCE	−0.50	–	Poznyak[81]
1991	n-Si	BP(–)	CVD	1 M H_2SO_4	∼0	–	+0.4 SCE	−0.6	–	Goossens[127]
2004	a-Si:Ge nip	ITO(–) /Fe_2O_3(–)	sputtering or spray pyrolysis	–	–	–	–	–	650	Miller[143]
2011	n-Si	TiO_2(2)/ Ir(3)	ALD	1 M H_2SO_4	0	8 h (5.1)	–	−0.22	532	Chen[119]
2011	n-Si	TiO_2(2)/ Ir(3)	ALD	0.4 M Na_2HPO_4, and 0.6 M Na_2HPO_4 and NaOH	7	8 h (5.1)	–	−0.28	565	Chen[119]
2011	n-Si	TiO_2(2)/ Ir(3)	ALD	1 M NaOH	14	24 h (15)	–	−0.20	555	Chen[119]
2011	*a*-Si	ITO(70)/ Co-oxide	–	1 M potassium borate	9.2	3 h (∼3.7)	−0.4 vs RHE	−1.63		Reece[77]
2012	n-Si	NiO_x(30)	sol−gel	buffered Na_2SO_4	7.25	30 min	–	−0.05	300	Sun[92]
2012	n-Si	Ti-Fe_2O_3(20)	CVD	NaOH-$NaHPO_4$ 1 M NaOH	13.8	–	+1.2 vs RHE	0	∼400	Jun[88]
2012	Ta_3N_5	CoO_x(–)	impregnation	1 M KOH	13.6	2 h (1)	+0.6 vs RHE	−0.60		Liao[106]

J. Phys. Chem. C XXXX, XXX, XXX−XXX
DOI: 10.1021/acs.jpcc.5b05976

Table 1. continued

year	base SC	coating (thickness, nm)[a]	deposition method	electrolyte	pH	stability, time (at J, mA cm^{-2})	E_{onset} vs ref (V)	E_{onset} vs OER (V)[b]	Vshift[c] (mV)	ref
2012	n-GaN	NiO	spin coating + annealing	1 M NaOH	14	110 h (0.5 mL $\cdot cm^{-2} \cdot h^{-1}$)	–	–	–	Hayashi[108]
2013	n-Si	Ni(2)	e-beam evaporation	1 M KOH	14	12 h (10)	–	−0.15	~500	Kenney[72]
2013	n-Si	Ni(2)	e-beam evaporation	0.65 M K-borate and 0.35 M Li-borate	9.5	80 h (10)	–	−0.05	~500	Kenney[72]
2013	n-Si	$NiRuO_x$(30)	sputtering	buffered Na_2SO_4	7.25	2 h (1)	–	−0.05	–	Sun[93]
2013	n-Si	MnO_x(10)	ALD	1 M KOH	13.6	~30 min (10)	–	−0.025	450	Strandwitz[68]
2013	$BiVO_4$	CoO_x(1)	ALD	0.1 M KOH	13	30 min (1.5)	+0.40 vs RHE	−0.83	–	Lichterman[44]
2013	$BaTaO_2N$	CoO_x(−), CoO_x + IrO_x(−), CoO_x + RuO_x(−)	calcination	0.1 M Na_2HPO_4(aq) and 0.1 M Na_2HPO_4(aq)	8	1 h (2)	–	−0.30	300	Higashi[104]
2013	TaON	$CaFe_2O_4$ + Co-Pi cocatalyst	electrophoretic deposition + calcination	0.1 M potassium phosphate buffer solution	11	3 h (0.5)	+0.6 vs RHE	−0.63	–	Domen[101]
2014	np^+-Si	ITO(100)/Au(5)/ ITO(100)/NiOx(−)	sputtering	1 M NaOH	14	2.5 h (10.8)	–	−0.05	388	Sun[80]
2014	np^+-Si	CoO_x(2)	ALD	1 M NaOH	13.6	24 h (30)	+1.1 vs RHE	−0.13	610	Yang[94]
2014	$BiVO_4$	FeOOH(−)/ NiOOH(−)	(photo) electrodeposition	phosphate buffer	7	50 h (2.6)	+0.2 vs RHE	−1.0	–	Kim[112]
2014	$BiVO_4$	$CaFe_2O_4$ (−) + Co-Pi cocatalyst (−)	electrophoretic deposition + calcination	0.1 M potassium phosphate buffer solution	7	2 h (2)	+0.3 vs RHE	−0.93	–	Kim[102]
2014	$BiVO_4$	TiO_2(1)/Ni(2)	ALD	0.1 M KOH	13	2 (1.4)	+0.6 vs RHE	−0.63	–	McDowell[109]
2014	n-CdTe	TiO_2(100-140)/ NiO_x(2)	ALD, e-beam evaporation	1 M KOH	14	100 h (20)	+0.7 vs RHE	−0.53	–	Lichterman[144]
2014	n-Si	TiO_2(3-143)/ Ni/ NiO_x(100)	ALD, e-beam evaporation	1 M KOH	13.7	–	+0.03 vs SCE	−0.16	430	Hu[49]
2014	np^+-Si	TiO_2(68)/ Ni/NiO_x(100) islands	ALD, e-beam evaporation	1 M KOH	13.7	>100 (35)	+0.12 vs SCE	−0.07	520	Hu[49]
2014	Ta_3N_5	ferrihydrite (−) + Co_3O_4 cocatalyst (−)	chemical bath deposition + calcination	1 M NaOH	13.6	6 h (5)	0.7 vs RHE	−0.53	–	Liu[103]
2014	np^+-Si	Ir/IrO_x(4)	sputtering	1 M H_2SO_4	0	18 h (25.5)	+1.05 vs RHE	−0.18	–	Mei[73]
2014	np^+-Si	Fe-treated NiO (50)	sputtering	1 M KOH	14	300 (15)	+1.05 vs RHE	−0.18	–	Mei[95]
2015	n-Si microwire	TiO_2(94)/ $NiCrO_x$(40)	ALD and Sputtering	1 M KOH	13.6	–	–	+0.07	180	Shaner[122]
2015	np^+-Si microwire	TiO_2(94)/ Ni(40)	ALD and sputtering	1 M KOH	13.6	2200 h (4.5)	–	−0.13	440	Shaner[122]
2015	np^+-Si	NiO_x(75)	sputtering	1 M KOH	14	1200 h (30)	–	−0.25	520	Sun[96]
2015	HTJ-Si	NiO_x(75)	sputtering	1 M KOH	14	200 h (34)	+0.95 vs RHE	−0.28	600	Sun[97]
2015	*a*-Si:H	NiO_x(75)	sputtering	1 M KOH	14	100 h (5.4)	+1.1 vs RHE	−0.12		Sun[97]
2015	$BiVO_4$	CoO_x (1 wt %)/NiO(~6)	bulk calcination/ALD	0.1 M KPi	7	16 h (2.5)	+0.4 vs RHE	−0.83	–	Zhong[113]
2015	n-CdTe	NiO_x(75)	sputtering	1 M KOH	14	1000 h (22.9)	+1.15 vs RHE	−0.07	440	Sun[97]

J. Phys. Chem. C XXXX, XXX, XXX−XXX DOI: 10.1021/acs.jpcc.5b05976

Table 1. continued

year	base SC	coating (thickness, nm)[a]	deposition method	electrolyte	pH	stability, time (at J, mA cm^{-2})	E_{onset} vs ref (V)	E_{onset} vs OER (V)[b]	Vshift[c] (mV)	ref
2015	np$^+$-Si	Ti(5)/TiO$_2$(100)/IrO$_x$	sputtering	1 M H_2SO_4 or 1 M $HClO_4$	0	60 h (23)	+1 vs RHE	−0.23	500	Mei[123]
2015	ZnO	Ta_2O_5 (–)	ALD	0.1 M KOH	13	5 h (0.8)	+0.5 vs RHE	−0.73	–	Li[145]
2015	np$^+$-InP	NiO$_x$(75)	sputtering	1 M KOH	14	48 h (20.8)	+0.85 vs RHE	−0.37	390	Sun[146]
2015	np$^+$-Si	$NiCo_2O_4$ (40)	sputtering	1 M KOH	14	72 h (30)	+1 vs RHE	−0.23	600	Chen[98]

[a]Outermost layer is the final layer listed, layer closest to the semiconductor is the first layer listed. [b]This would be the voltage vs the thermodynamic potential (as calculated); negavie means more negative past the thermodynamic potential. [c]This would be the voltage shift from the dark electrocatalysis on a metal or degenerate electrode that are comparable to the electrocatalytic behavior of as-reported photoanodes. [d](--) data not specified or parameter not reported. (w) Effective water oxidation not demonstrated. (v) Possibly photocorrosion.

calomel electrode (SCE, 0.241 V vs NHE at 25 °C), the saturated silver/silver chloride (Ag/AgCl, 0.197 V vs NHE at 25 °C), or the mercury/mercury oxide (Hg/HgO with 1.0 M NaOH, 0.098 V vs NHE at 25 °C) electrodes because these references are conveniently used for PEC experiments performed in aqueous media. These reference potentials can be converted to the RHE scale by explicitly measuring the RHE potential in the electrolyte of interest[67] or by an arithmetic conversion using the known potential differences between the reference electrode and the RHE potential. We note, however, that due to nonzero temperature coefficients, junction potentials, and the tendency for reference electrode potentials to drift over time, it is always preferable to provide an explicit calibration to the RHE scale when possible. In Table 1, when potentials other than RHE were reported, a specified arithmetic conversion has been performed to calculate the potential vs RHE, based on the solution pH, but the onset potential is also provided with respect to the reported reference electrode.

Summary of Available Library of Stable Materials. The corrosion stability of oxide coatings and semiconductor light absorbers is generally referenced to the Pourbaix diagrams (*vide supra*). Many metals form insoluble oxides and self-passivate under water oxidation potentials (E > 1.23 V vs RHE) and certain pH conditions, by being biased into the "passivation" region (Figure 2).[25] However, under certain electrochemical and pH conditions, many oxides form soluble species, resulting in film destruction/dissolution. Due to their insolubility over certain ranges of pH, but without considering their electronic transport properties, the following metal oxides can be considered as candidates for photoanode protective coatings over some appreciable range of pH values: TiO_2, ZrO_2, HfO_2, SnO_2, In_2O_3, FeO_x, MnO_x, NiO_x, CoO_x, WO_3, ZnO, Ta_2O_5, NbO_x, Al_2O_3, MgO, SiO_2, BiO_x.[26] Thermodynamic stability (through the formation of insoluble oxides/hydroxides), however, is not a sufficient condition for corrosion protection. For example, thin layers of NiO_x, CoO_x, and MnO_x may become porous during passage of current and may thus allow for eventual permeation of electrolyte to the underlying semiconductor surface.[61,68]

3.2. Protection of Photoanodes for Water Splitting.

3.2.1. Metals and Metal Silicide Protective Layers. Although metals and metal silicides absorb or reflect considerable light, thin layers or sparse coverages allow for their use as protective and functional films. An additional drawback of metals is that metal/semiconductor Schottky contacts generally have large majority-carrier-based recombination currents due to thermionic emission processes at the semiconductor/metal interface and thus produce small photovoltages.[69] Attempts to protect n-type GaP (n-GaP) and n-type Si (n-Si) photoanodes in the late 1970s relied on thin layers of Au, Pd, and Ag films deposited by electron-beam evaporation or sputtering.[70] Later, Wilson et al. revisited such a metal-layer stabilization strategy by studying a Au/n-GaP combination.[71] The energy-band diagram indicated that the metal overlayer formed a buried Schottky junction with n-GaP; hence this metal coating contacted the electrolyte (similar to Figure 5b).

Recently, a 2 nm Ni layer was reported to stabilize n-Si photoanodes in 1 M KOH (pH = 14) for 12 h as well as in borate buffer (pH = 9.5) for 80 h,[72] with an initial current density of 10 mA cm^{-2}. The proposed energy-band diagram suggests that, upon contact with liquid electrolytes, a thin Ni layer on Si forms a buried Schottky junction with a higher barrier height than a thick Ni layer on Si. This hypothesis is

DOI: 10.1021/acs.jpcc.5b05976
J. Phys. Chem. C XXXX, XXX, XXX−XXX

supported by the observation of a photovoltage under simulated 1 Sun illumination of 500 mV, which is larger than the V_{oc} observed for conventional n-Si/Ni junctions with thicker Ni layers. NiO_x can become porous during prolonged water oxidation, which makes this method potentially problematic in terms of the film permeability. The anodization depth is also critical to the protection capabilities of the metal films and is a function of several parameters including the current density, potential, temperature, and electrolyte composition.

Chorkendorff and co-workers[73] used a 4 nm Ir layer to stabilize Si p^+−n junction photoanodes (n-type bulk with a p^+ emitter at the surface) in 1.0 M H_2SO_4 for 18 h at an average current density of 25.5 mA cm^{-2}. They posited that the operative semiconductor/electrolyte interface involved a buried photovoltaic junction in contact with metallic Ir serving as an ohmic contact as well as a water-oxidation catalyst. The XPS depth profiling data indicated that the Ir anodized to a depth of less than 4 nm and maintained protection of the Si photoanodes. These results are encouraging because even slower anodization of Ir is expected in alkaline media.[74] The coating thus needs to be sufficiently thin to obviate obscuration of incident light yet sufficiently thick to prevent anodization that leads to porous protective and catalytic coatings under operating conditions.

3.2.2. Metal Oxide Protective Layers. Due to their chemical stability and optical transparency, metal oxides represent the most common class of thin layers used for photoanode protection. Due to the abundance of research conducted with this class of materials, we have further subdivided this class into the following categories: (1) catalytically inactive transparent conductive oxides (TCO), (2) catalytically active metal oxides, and (3) redox-inactive metal oxides.

3.2.2.1. Catalytically Inactive TCO Protective Layers. Catalytically inactive TCOs, such as Sn-doped In_2O_3 (ITO), SnO_2, or F- or Sb-doped SnO_2, resist corrosion in neutral or near-neutral pH aqueous electrolytes but corrode at extreme pH values. These protective coatings either form Schottky barriers or create ohmic contacts to underlying solid-state photovoltaic junctions. TCO−semiconductor Schottky contacts are generally subject to high recombination velocities and therefore generally produce low V_{oc} values. However, when a PV junction is decorated with a TCO layer, high V_{oc} values can still be obtained.

ITO layers have been used to protect a wide variety of semiconductors, including n-Si, n-GaAs, a GaP/amorphous Si/crystalline Si tandem,[75] triple-junction amorphous Si, and Si−Ge alloy solar cells.[76−79] Due to a low catalytic activity toward oxygen evolution, ITO surface layers are usually further functionalized with catalysts such as RuO_2, Fe_2O_3, and Co-oxide. ITO-coated triple-junction amorphous Si solar cells have shown >3 h of stability at a photocurrent density of ∼3.7 mA cm^{-2} in 1.0 M potassium borate buffer (pH = 9.2) but showed <30 min of stability in 0.10 M KOH (pH = 13), likely because In_2O_3 is soluble in aqueous media with high pH values.[26,77] n-Si coated with 40 nm of ITO as well as with a RuO_2 cocatalyst showed an onset of photoanodic current at 0.1 V negative of the water-oxidation potential in buffered pH = ∼ 12.5 NaOH(aq), but neither oxygen yields nor long-term stability data were reported.[76] Recently, an ITO/Au/ITO stack was deposited on a Si p−n junction and produced 2.5 h of photoanodic stability in 1.0 M NaOH (pH = 14).[80] Most TCOs are n-type semiconductors and thus do not generally form high barrier-height contacts to many n-type semiconductor absorbers, due to a close alignment of the Fermi levels of the TCO to the conduction band of the semiconductor. Therefore, many attempts to realize high performance for water oxidation have used PV junctions coated with TCO protective films, as described above.

Chromium-containing oxides have been used to stabilize oxygen-evolving photoanodes, perhaps motivated or justified by the utility of chromia scales in protecting stainless steels. For example, Cr_2O_3 films deposited by CVD at 500 °C have been used to stabilize n-Si photoanodes in 1.0 M H_2SO_4, with a photovoltage of 0.5 V.[81] A mixed oxide containing Cr_2O_3:TiO_2:SbO_x deposited on the Cr_2O_3 was reported to stabilize an n-Si photoanode in an electrolyte consisting of 1 M H_2SO_4 and 1 M isopropanol. However, the measured photocurrent diminished continually over 20 h, and the effect of the added isopropanol was not explained. It is possible that the measured current was due to isopropanol oxidation, rather than oxidation of water to produce O_2(g).

3.2.2.2. Catalytically Active Metal Oxide Protective Layers. Catalytically active transition-metal oxides and silicates have also been widely explored as protective coatings. This strategy attempts to exploit a possible dual function of the metal oxide film: protection and catalysis. Bockris and co-workers[82] used Pt-doped SiO_2 (SiO_2 electrochemically grown on Pt-coated Si surfaces) formed by photoanodic oxidation to stabilize n-Si photoanodes in 0.5 M H_2SO_4 (pH = ∼ 0) for 100 h at a photocurrent density of 1 mA cm^{-2}. Electron-beam-evaporated Fe_2O_3 has also been used to stabilize n-Si and showed an onset of photoanodic current at ∼0.4 V vs SCE (∼1.3 V vs RHE) in 0.1 M KOH,[83] indicating a low photovoltage and almost no power saved by the n-Si photoelectrode when coated with iron oxide. Iron oxide coatings on n-Si photoanodes have been further investigated in terms of structure[84] and performance in contact with electrochemically reversible redox couples[85] as well as in contact with alkaline media with[86] and without[83,87−89] methanol. Jun et al.[88] used hematite (α-Fe_2O_3) mixed with 4% Ti to cover an n-Si electrode surface and observed a photoanodic current onset of ∼1.1 V vs RHE in 1 M NaOH (pH = 13.8). In this study, a potential shift of ∼ −0.55 V between an ITO electrode coated with iron oxide in the dark relative to an n-Si photoanode coated with iron oxide in the light can be inferred, indicating an appreciable photovoltage produced by this type of stabilized Si photoanode.

MnO_x coatings deposited by chemical-bath deposition, along with an electrodeposited noble-metal layer, have shown promise.[90,91] MnO_x-coated GaAs and Si showed stable anodic current for 80 min (at 11 mA cm^{-2}) in 0.5 M NaOH and 60 min (at 1.2 mA cm^{-2}) in 0.5 M K_2SO_4, respectively. In both studies, electrodeposited noble metal layers of Pd or Pt were used prior to the deposition of MnO_x, making it unclear if the noble metal played a role in protection. Strandwitz et al.[68] showed that manganese oxide deposited using ALD stabilized n-Si without noble metal layers when the electrodes were contacted by the electrochemically reversible, one-electron ferri-/ferrocyanide redox couple, and they also showed that the protected n-Si photoanode oxidized hydroxide for ∼30 min at an average photocurrent density of 24 mA cm^{-2} in 1 M KOH(aq). A photovoltage of 0.45 V was observed for MnO_x-coated Si photoanodes, and the light-limited current density indicates that the MnO_x coating partially absorbs incident illumination. It was hypothesized in this case that electrochemically induced porosity was ultimately responsible for failure of the protective film.[68]

DOI: 10.1021/acs.jpcc.5b05976
J. Phys. Chem. C XXXX, XXX, XXX−XXX

Other first-row transition metal oxides have stabilized photoanodes under neutral and alkaline conditions. Recently, NiO_x, CoO_x, and $NiRuO_x$ protective layers comprised of OER catalysts have been used for this purpose.[72,92−94] Sol−gel deposited NiO_x on n-Si showed 4 h of photoanodic water oxidation in phosphate-buffered Na_2SO_4(aq) at an initial current density of 7 mA cm^{-2}, with the current density decreasing to 1 mA cm^{-2} over several days of continuous operation (pH = 7.25).[92] Sputtered $NiRuO_x$ and ALD-grown CoO_x stabilized n-Si in 1 M KOH(aq) for 2 h (at 1 mA cm^{-2}) and for 24 h (at 10 mA cm^{-2}), respectively. Chorkendorff and co-workers recently reported that Fe-treated NiO thin films with a Ti underlayer protected Si-based photoanode assemblies for water oxidation for 300 h at 1.3 V vs RHE, although the current declined continuously during the reported stability test.[95] Sun et al. reported that sputtered NiO_x films protected heterojunction-Si (*a*-Si/c-Si), amorphous Si (*a*-Si:H), n-CdTe, and buried junction np^+-InP for water oxidation for up to 1200 h in 1 M KOH, while the photoanodes were operated continuously at their light-limited current densities.[96,97] Electrochemically induced porosity that is common in many metal oxide coatings was not considered to be an issue for these NiO_x coatings. Chen et al.[98] investigated p-type $NiCo_2O_4$ as a protection layer for Si. *Inssitu* Raman spectroscopy was used to show that the metal oxide was structurally stable under electrochemical cycling. The photoelectrochemical performance was similar to that of the NiO_x-coated photoanodes discussed above. Stability testing was conducted for 72 h, but analysis of the electrolyte for corrosion products suggested a much longer lifetime.

Oxide and Nitride Absorbers. Metal-oxide OER catalysts have also been used to improve the stability of oxide, nitride, and oxynitride light-absorbing materials under photoanodic conditions and warrant comment here. The general expectation is that nitride-based absorbers are more stable than other nonoxides. However, oxides, nitrides, or oxynitrides are not always stable and require cocatalysts or protection strategies to improve their stability. Domen and co-workers showed that IrO_2 and CoO_x particles could be sparsely deposited on TaON by chemical-bath deposition or electrophoretic deposition, respectively, and both types of TaON photoanodes exhibited improved stability, 1−2 h in buffered 0.1 M Na_2SO_4 electrolyte (pH = 6).[99,100] An onset potential of 0.63 V negative of the water oxidation potential was observed from this 2.7 eV band gap semiconductor. By forming a heterojunction, calcium ferrite (p-$CaFe_2O_4$) modified TaON or $BiVO_4$ photoanode showed improved performance for water splitting as compared to the same material without a surface coating.[101,102] Li et al. reported that a ferrihydrite ($Fe_5HO_8{\cdot}3H_2O$) layer protected a Ta_3N_5 photoanode against photocorrosion for >6 h, while the bare Ta_3N_5 only operated for several minutes under the same conditions. The ferrihydrite was hypothesized to be a hole storage layer, which captured and transmitted the photogenerated holes readily to the electrolyte or to the Co_3O_4 catalyst.[103] $BaTaO_2N$ treated with preloaded CoO_x particles and postloaded with RhO_x, along with a necking treatment that involved impregnating a $TaCl_5$ solution followed by treatment with H_2, showed at least 1 h stability for water oxidation in pH = 8 phosphate buffer.[104] Barium-doped tantalum nitride nanorod photoanodes exhibited up to 1.5% solar energy-conversion efficiency with a faradaic efficiency of unity for 100 min at pH 13, when modified with cobalt phosphate as the catalyst.[105] Similarly, Ta_3N_5 was stabilized in 1 M KOH for 2 h using surface-impregnated CoO_x particles, and the electrode showed an onset of oxygen evolution at 0.6 V vs RHE under visible (λ > 420 nm) illumination.[106] n-GaN showed improved stability in 1 M NaOH for up to 100 h using a surface-located NiO cocatalyst.[107,108]

The relatively narrow band gap metal oxide semiconductor, $BiVO_4$, is only stable anodically at pH = ∼7 in contact with electrochemically reversible redox couples. Consistently, $BiVO_4$ only lasts for a few cyclic voltammetric scans in pH > 13 before the material dissolves.[109] However, the photoanodic stability of $BiVO_4$ can be improved by deposition of a cocatalyst of Co-phosphate and FeOOH.[110,111] Lichterman et al.[109] showed that ALD-grown CoO_x can improve the stability of $BiVO_4$ in 0.10 M KOH (pH = 13) to >0.5 h, and Choi and co-workers[112] showed that a photoelectrodeposited FeOOH/NiOOH catalyst layer stabilized $BiVO_4$ surfaces in phosphate buffer (pH = 7) for ∼50 h. Very recently, Domen[113] and co-workers found that further deposition of an ultrathin *p*-type NiO layer by ALD on the $CoO_x/BiVO_4$ photoanode made by the particle transfer method tripled the photocurrent density and rendered the photoanode stable for at least 16 h at pH 7, with a light-limited photocurrent density of 2.5 mA cm^{-2}. The photocurrent onset potential of $BiVO_4$ electrodes was 0.4 V vs RHE, a −0.83 V shift from the formal potential for water oxidation from this 2.3 eV band gap material. In this work, the *in situ* formed NiOOH together with CoO_x were responsible for the improved water oxidation activity and formed a buried junction between the p-NiO and the n-$BiVO_4$.[113]

3.2.2.3. Catalytically Inactive, Wide Band Gap Metal Oxide Protective Layers. Catalytically inactive, chemically stable, wide band gap metal oxides have been investigated as barrier layers to stabilize photoanode surfaces, and such barrier layers may obviate the drawback of electrochemically induced porosity. Parsons and co-workers observed that the passivating behavior of TiO_2, ZnO, and Al_2O_3 thin films led to reduced photocorrosion of Si but was accompanied by a significant reduction in hole conduction.[114] Often, an insulating or wide band gap protection layer like TiO_2 behaves as a barrier to transport of photogenerated holes, due to the valence band offset between TiO_2 and nonoxide semiconductors.[115] A clear demonstration of the hole barrier introduced by wide band gap oxides was shown by the decline in photocurrent on a TiO_2 photoelectrode that accompanied the deposition of an insulating MgO film.[116] In this case, the TiO_2 was the semiconductor being covered by the MgO. Although the TiO_2 did not require protection, the study produced a clear demonstration of inhibited hole conduction. Within oxynitride-based absorbers, a necking treatment consisting of $TiCl_4$ and $TaCl_5$ impregnation, followed by annealing, resulted in the formation of TiO_2 and Ta_2O_5 between light absorber particles and increased the photoelectrode stability and performance.[104,117,118]

One approach to transport holes through the blocking layer is by tunneling or trap-assisted tunneling. Recently, this strategy has been demonstrated using a 2 nm thick TiO_2 film grown by ALD with a thin Ir film overlayer that has stabilized n-Si photoanodes for 8 h in 1.0 M H_2SO_4, phosphate buffer (pH = 7), or 1 M NaOH.[119,120] Similarly, a ∼1 nm ALD-grown TiO_2 film was used to stabilize n-ZnO in 0.1 M KOH (pH = 13) for 3 h of water oxidation.[121] In these cases, conduction through the crystalline TiO_2 layer was attributed to hole tunneling, which limits the film thickness to ∼2 nm.[69]

DOI: 10.1021/acs.jpcc.5b05976
J. Phys. Chem. C XXXX, XXX, XXX−XXX

Recent studies of ALD-grown TiO_2 protective films on Si have shown effective hole transport even with TiO_2 layers that are too thick to facilitate effective hole tunneling,[120] in support of previous theoretical work suggesting this might be possible.[48] The amorphous TiO_2 coating was grown by ALD using tetrakisdimethylamido titanium (TDMAT) and was found to stabilize Si, GaAs, GaP, and CdTe in 1.0 M KOH(aq) for >100 h, with islands of NiO_x as the OER cocatalyst.[44,49] Although this TiO_2 film is chemically stable, identification of the mechanism of hole conductivity requires further investigation. This amorphous TiO_2 coating has also stabilized structured, high-aspect-ratio light absorbers such as Si microwires for >2200 h of continuous operation under water oxidation conditions in 1.0 M KOH.[122] Such an amorphous TiO_2 coating can also stabilize $BiVO_4$ but with a thickness of ~1 nm, where tunneling of photogenerated charge carriers is possible.[109] In all of these studies, the TiO_2 was formed by the ALD using TDMAT as a Ti precursor, which may be responsible for the unique, "leaky" electronic behavior, possibly due to nitrogen content from the amido-based precursor and/or Ti^{3+}. Regardless of the chemical origins of such electronic transport, such a scenario was proposed by Campet, and an adapted band diagram is shown in Figure 6 that may explain the behavior of these TiO_2-coated electrodes.[48] An alternative explanation involves transport of electrons through TiO_2 which essentially acts as an ohmic contact between Ti and a Pt catalyst in an np^+-Ti−TiO_2−Pt stack.[123] The TiO_2 in this study was deposited using sputtering, and it was claimed that it did not possess states that would yield a "leaky" TiO_2 layer. However, this work also utilized a metal (5 nm Ti) intermediate layer between the TiO_2 and Si absorber (rather than a direct TiO_2−Si contact) which functioned like a tunnel junction for recombination of holes in the p^+ Si and electrons in TiO_2. The Ti layer was said to have formed a high barrier height (yet ohmic) contact to the p^+ emitter and an ohmic contact to the TiO_2. The authors also specifically studied the transport from the p^+ Si emitter into a Ti Schottky contact as a function of the emitter doping density.

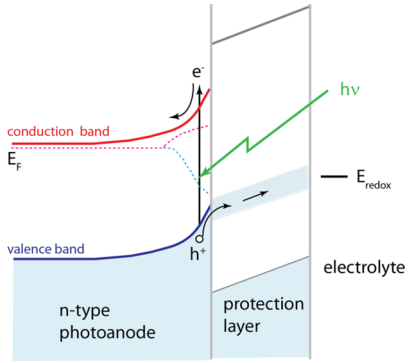

Figure 6. Hole conduction through a thick (>2 nm) protective layer, adapted from Campet et al.[48] A "mini" band in the wide band gap protective layer obviates hole blockage that would otherwise occur due to a large mismatch in the energy levels of the valence band of the semiconductor and the oxide protection layer. Used with permission under Creative Commons Attribution License, Copyright 1989 Hindawi Publishing Group.

3.2.3. Nitride, Phosphide, and Boride Protective Layers. Nitride-based compounds (e.g., GaN, TaN_x) have generally shown better stability for PEC water oxidation than is obtained using Si, Ge, or compound arsenide semiconductors,[124,125] but reports describing the use of nitrides as protective films are not common. Boron phosphide (BP with 1:1 ratio of boron and phosphorus) has been grown on n-Si and n-GaAs to increase the photoanode stability but was initially only examined in contact with electrochemically reversible aqueous couples.[126] An n-type BP layer grown epitaxially by CVD methods using BBr_3 and PBr_3 as precursors in a stream of dry H_2 as carrier gas yielded improved photoanodic and cathodic stability on n-Si and p-Si, respectively.[127] The BP-protected n-Si photoanode showed a photoanodic current onset of 0.4 V vs SCE, and neither light-limited photocurrent densities nor the extent of stability under operation were reported. In contrast, the BP-protected p-Si photocathode showed more than 1000 h of continuous operation at a photocurrent density of 15 mA cm^{-2}. No quantitative yield of O_2 and H_2 was reported for either BP-protected n-Si photoanodes or p-Si photocathodes. As is further discussed below, enhanced stability could be due to alloying of the B- or P-based components of the film with the Si.

3.3. Protection of Photoanodes for Halide Splitting. Table 2 presents reports of thin-layer protection for photoanodes performing the oxidation of halides. These reactions generally proceed more readily than oxygen evolution due to more facile interfacial kinetics for the oxidative half-reactions of the halides relative to water oxidation. In the early 1980s, Bard and co-workers used noble metals to stabilize Si photoanodes for halide oxidation.[128] A Pt-modified n-Si photoanode showed a photovoltage of 0.40 V, which is consistent with a Schottky barrier formed between Pt and n-Si. The light-limited photocurrent density was 14 mA cm^{-2} under 65 mW cm^{-2} of simulated solar illumination. Nakato et al.[129] attempted a similar strategy using buried junction np^+-Si photoanodes and obtained a photovoltage of 550 mV and a photocurrent density of 12 mA·cm^{-2}. Islands of Pt particles were shown to protect n-Si photoanodes in a 4.8 M HBr/0.03 M Br_2 electrolyte.[130]

In addition to metals and silicides, conductive oxide coatings such as ITO, SnO_2, Sb-doped SnO_2, TiO_2, Fe_2O_3, and WO_3 have been shown to exhibit stable photoelectrochemical behavior in conjunction with n-Si photoanodes under halide oxidation conditions.[76,131−134] Both ion-beam sputtered ITO on n-Si with a RuO_2 cocatalyst and CVD-grown SnO_2 on n-Si with a Pt cocatalyst have shown 20 h of stability in either a Cl_2/Cl^- electrolyte (pH = 6.6) or in a I_3^-/I^- electrolyte (pH = 1.5), respectively.[76] Yano et al.[134] reported that thin layers of electron-beam evaporated TiO_2, Fe_2O_3, or WO_3 stabilized np^+-Si junctions for iodide oxidation, and a TiO_2-stabilized buried junction np^+-Si photoanode exhibited V_{oc} = 580 mV and 330 h of stability for the oxidation of fuming HI.

Boron-alloyed Si surfaces also have shown stability for halide oxidation. In one case, an np^+-Si junction with a heavily B-enriched surface was formed by drop casting a saturated methanol solution of boron trioxide (BO_3) onto Si surfaces, followed by annealing at 1000 °C for 2 h in air.[135] During oxidation of 57% fuming HI, such a boron-alloyed Si surface showed 7 h of photoanodic stability at 15 mA cm^{-2} with a V_{oc} = 300 mV. With a Pd catalyst overlayer, the PEC performance improved to yield V_{oc} = 650 mV while providing 7 h of stability at 32 mA cm^{-2} of photoanodic current density. In this case, as well as in the BP case described previously for OER and HER, the well-known "etch-stop" mechanism could be responsible for the stability of these layers. Boron-alloyed layers are commonly exploited to produce etch stop layers during micromachin-

DOI: 10.1021/acs.jpcc.5b05976
J. Phys. Chem. C XXXX, XXX, XXX−XXX

Table 2. Photoelectrosynthetic Systems for Halide Oxidation[a]

year	base SC	coating (thickness, nm) (a)	deposition method	electrolyte	pH	stability, time (at J, mA cm^{-2})	E_{onset} vs ref (V)	V_{oc} (mV)	ref
1982	n-Si	CuPc (150)	coating, passivated electrode	0.2 M NaI/0.004 M I_2/ 0.5 M Na_2SO_4	--	30 s (0.2)		--	Leempoel[147]
1982	n-Si	CuPc (80)	coating, passivated electrode	1 M NaI/0.004 M I_2	--	500 s (9)	−0.1 V vs SCE	--	Leempoel[147]
1982	n-Si	Surface doped n-Si (−)	drop-cast followed by diffusion	57% HI	--	7 h (15)	−0.25 V vs SCE	300	Nakato[135]
1982	n-Si	Surface doped n-Si (−)	drop-cast followed by diffusion	57% HI	--	7 h (32)	−0.6 V vs SCE	650	Nakato[135]
1983	n-Si	Pt silicide (∼4)	flash evaporation	1 M NaI, 0.1 M I_2	--	--	−0.1 V vs SCE	400	Fan[128]
1983	n-Si	Pt silicide (∼4)	flash evaporation	0.5 M Na_2SO_4, 1 M NaBr	--	8 h (4)	+0.4 V vs SCE	--	Fan[128]
1983	n-Si	n-Si(Ir) (−)	flash evaporation	11 M LiCl	5	3 h (7)	+0.7 V vs SCE	--	Fan[128]
1983	n-Si	RuO_2-modified n-Si(Ir) (∼4)	flash evaporation	11 M LiCl	5	7 d (9)	+0.6−0.7 V vs SCE (estimated)	--	Fan[128]
1983	n-Si	ITO (∼40)	ion beam sputtering	15 M LiCl/0.05 M Cl_2	∼6.6	20 h (14.3) in 5 M NaCl	+0.7 V vs SCE	160	Hodes, Thompson[76,131]
1983	n-Si	SnO_2/Ru (80)	spray/CVD	3 M NaCl/sat. Cl_2 system	--	--	--	340	Decker[132]
1983	n-Si	SnO_2 (80)	spray/CVD	3 M NaCl/sat. Cl_2 system	--	--	--	470	Decker[132]
1983	n-Si	SnO_2/Sb (80)	spray/CVD	3 M NaCl/sat. Cl_2 system	--	--	--	460	Decker[132]
1984	n-Si	Polyacetylene (−)	polymerization	0.5 M LiI, 10 mM I_2 in 11 M LiCl	--	23 h (2.2)	−0.2 V vs SCE	400	Simon[137]
1985	np^+-Si	Pt silicide (<5)	E-beam evaporation followed by annealing and HF etching before PEC	7.6 M HI/0.05 M I_2	--	4500 h (12)	−0.55 V vs I_3^-/I^-	550	Nakato[129]
1985	np^+-Si	TiO_2 (3−20)	E-beam evaporation	7.6 M HI/0.03−0.05 M I_2	--	330 h (16)	−0.57 V vs SCE	580	Tsubomura[134]
1985	np^+-Si	Fe_2O_3 (3−20)	E-beam evaporation	7.6 M HI/0.03 M I_2	--	--	−0.53 V vs SCE	540	Tsubomura[134]
1985	np^+-Si	WO_3 (3−20)	E-beam evaporation	7.6 M HI/0.03 M I_2	--	--	−0.53 V vs SCE	540	Tsubomura[134]
1986	n-Si	SnO_2 (40−50)	CVD	0.4 M KI/0.00075 M I_2, 0.5 M $NaSO_4$	1.5	20 h (19 to 17)	--	549	Belanger[133]
1992	n-Si	Pt islands/SiO_x (−)	vacuum deposition followed by alkali-etching	4.8 M HBr/0.03 M Br_2	--	--	--	660−680	Nakato[130]
2004	n-Si	nanodot Pt (−)	electrodeposition	8.6 M HBr + 0.05 M Br_2	--	--	−0.68 V vs I_3^-/I^-	680	Takabayashi[139]
2004	n-Si	methyl-n-Si + Pt (−)	methylation and electrodeposition	8.6 M HBr + 0.05 M Br_2	--	3 h (24)	--	--	Takabayashi[139]
2004	n-Si	methyl-n-Si + Pt (−)	methylation and electrodeposition	7.6 M HI + 0.05 M I_2	--	24 h implied by XPS data	−0.55 V vs I_3^-/I^-	550	Takabayashi[139]
2013	n-Si	PEDOT:PSS (20)	spin coat	8.4 M HBr	<0	7 (10)	+0.3 V vs Pt (in 8.4 M HBr)	380	Mubeen[138]
2013	n-Si	PEDOT:PSS (20)	spin coat	HI	∼2	6 (7)	−0.3 V vs Pt (in pH2 HI)	380	Mubeen[138]

[a](--) data not specified or parameter not reported.

DOI: 10.1021/acs.jpcc.5b05976
J. Phys. Chem. C XXXX, XXX, XXX−XXX

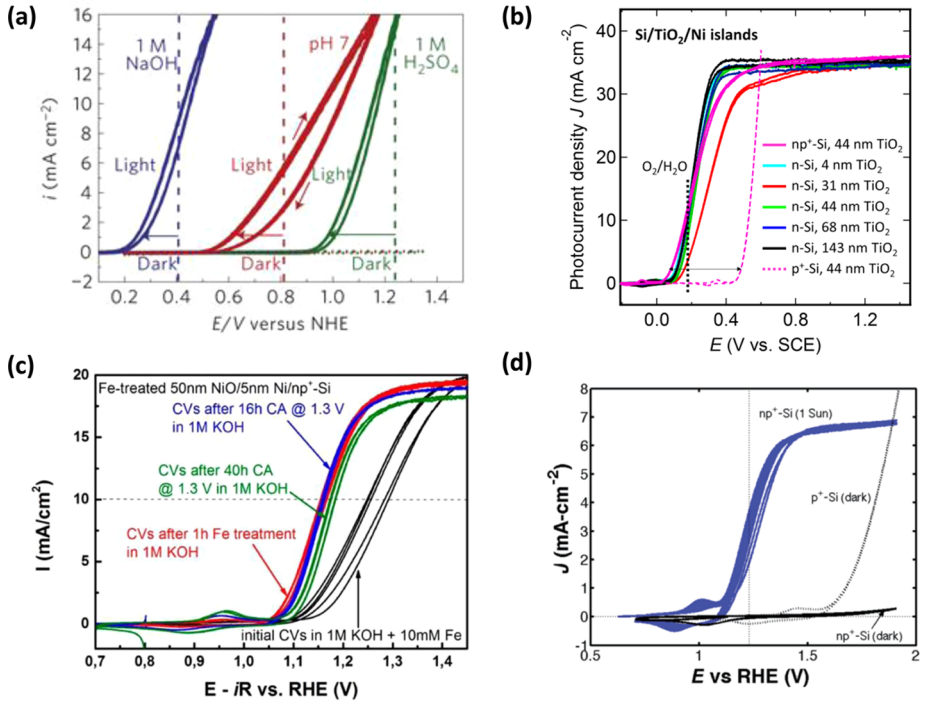

Figure 7. State-of-the-art performance of thin-layer protected Si photoanodes. The light absorber/protective coating/catalyst compositions are (a) n-Si/2 nm TiO_2/Ir. Reprinted by permission from Macmillan Publishers Ltd.: Nature Materials (ref 119), Copyright 2011. (b) n-Si or np^+-Si/4−143 nm TiO_2/Ni islands. Reproduced with permission from The American Association for the Advancement of Science, 2014 (ref 49). (c) np^+-Si/Fe-treated 50 nm NiO. Reproduced with permission from the American Chemical Society (Ref 95). (d) np^+-Si wires/94 nm TiO_2/$NiCrO_x$. Reproduced from ref 122 with permission from The Royal Society of Chemistry.

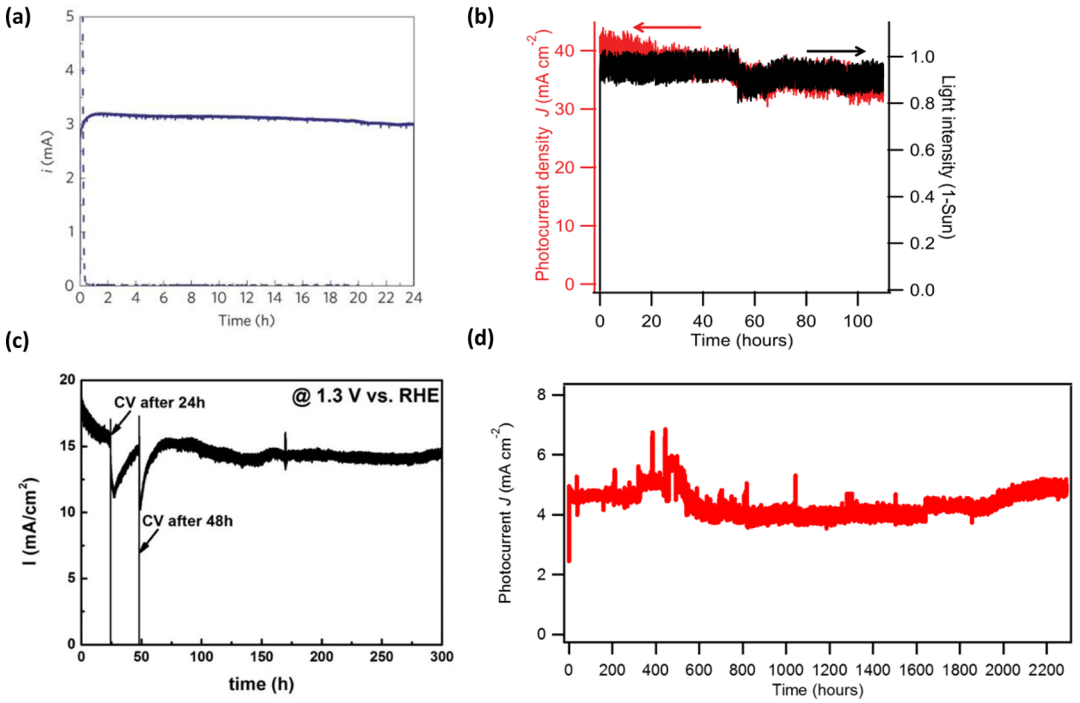

Figure 8. State-of-the-art stability of the corresponding thin-layer protected Si photoanodes in Figure 7. The corresponding photoanode structures are: (a) n-Si/2 nm TiO_2/Ir. Reprinted by permission from Macmillan Publishers Ltd.: Nature Materials (ref 119), Copyright 2011. (b) n-Si or np^+-Si/4−143 nm TiO_2/Ni islands. Reproduced with permission from The American Association for the Advancement of Science, 2014 (ref 49). (c) np^+-Si/Fe-treated 50 nm NiO. Reproduced with permission from the American Chemical Society (ref 95). (d) np^+-Si wires/94 nm TiO_2/$NiCrO_x$. Reproduced from ref 122 with permission from The Royal Society of Chemistry. The black curve in (b) indicates the monitored illumination intensity as a function of time.

DOI: 10.1021/acs.jpcc.5b05976
J. Phys. Chem. C XXXX, XXX, XXX−XXX

ing,[136] and the high conductivity of these layers may also allow for favorable electron-transfer properties and photoactive barrier formation in water-splitting devices.

Various organic films also show promise for protection against corrosion and catalysis for halide oxidation. Wrighton and co-workers[137] showed that polyacetylene-coated n-Si [n-Si/$(CH)_x$] stably oxidized I_3^-/I^- for 23 h at a photocurrent density of 2.2 mA cm^{-2}. Similarly, McFarland and co-workers[138] have shown that a PEDOT:PSS-coated n-Si photoanode can oxidize HBr and HI for 7 and 6 h, respectively. The photovoltage of such polymer/Si junctions was 380−400 mV. However, the measured light-limited photocurrent density from PEDOT:PSS-coated n-Si photoelectrodes was 7−10 mA cm^{-2} because PEDOT:PSS coatings strongly absorb incident illumination. A methylated n-Si(111) surface with electrodeposited Pt islands showed a photovoltage of 550 mV in contact with I_3^-/I^- redox and showed a photoanodic stability of 3 h at 24 mA cm^{-2} in contact with the Br_2/Br^- redox couple.[139] In contrast, Pt-electrodeposited and hydrogen-terminated n-Si and bare hydrogen-terminated n-Si showed an immediate photocurrent drop within <1 h.

3.4. Summary and Perspectives of Photoanode Protection. Figure 7 and Figure 8 display cyclic voltammetric and chronoamperometric data, respectively, for some of the best-performing demonstrations of protection via tunnel-oxide conduction, "leaky" defect-state conduction, and doped TCO conduction. Each of these strategies yields excellent performance in terms of photocurrent and photovoltage, as well as continued OER activity for periods of many hours. To date, various oxide coatings have resulted in both high performance and $>10^2$ h of stability for protected photoanodes. The ALD-grown amorphous TiO_2 strategy has exhibited the best protection to date for a variety of materials for the longest time periods at relevant current densities (~2200 h, ~5 mA cm^{-2}), but it may not be the only or best choice as a protective coating. NiO_x protective coatings have shown >1000 h stability consistently for self-passivating materials (e.g., Si and CdTe) with planar configuration. Therefore, one future direction in photoanode stabilization would focus on catalytically active oxides (NiO_x, CoO_x, and mixed $NiFeO_x$), inactive metal oxides (ZnO, ZrO_2, HfO_2, and BiO_x), nitrides (GaN, TaN_x), and carbides (TaC, TiC, and ZrC) that may be doped or engineered with defect states within the band gap so that they allow hole transport in an analogous fashion to amorphous ALD TiO_2. The successful implementation of this approach in general will benefit from a systematic understanding of the origin and energetics of defect states and conduction mechanisms in these stable materials.

Second, the combination of catalytically active oxides and catalytically inactive barrier layers provides an approach to separate the functions of protection/conductivity (e.g., TiO_x) and catalysis (e.g., NiO(OH)) and represents an immediate engineering approach to obtaining additional improvements in the lifetime of stabilized photoanodes. This strategy may avoid issues related to electrochemically induced porosity in the protective film.

A few remaining gaps still exist for photoanode stabilization. n-Si has been stabilized for >1000 h in either alkaline or acidic electrolytes, but stability with high photovoltage and photocurrent without using a buried junction has not been reported. n-Si/TiO_2/Ir configurations have shown 560 mV photovoltages,[119] whereas other combinations of n-Si and protective coatings produce photovoltages <450 mV. For GaAs, no strategies other than ALD-grown amorphous TiO_2 have demonstrated stability, and the photovoltages of such systems need to be improved by interfacial engineering. For n-InP and n-CdTe, catalytically active coating strategies have been demonstrated, but interfacial engineering would be beneficial to improve the energy-conversion performance of such devices. For Ta_3N_5, stability has been improved to a few hours, but long-term stability requires further coating development.

4. PROTECTION OF PHOTOCATHODES

4.1. Overview. Although early experiments in the field of solar-driven water splitting emphasized the use of wide band gap, n-type oxide absorbers, p-type semiconducting materials can also facilitate solar-assisted hydrogen evolution, provided that the absorbers are coupled to suitable HER electrocatalysts.[148] The early demonstrations of PEC-based hydrogen evolution did not include explicit efforts to protect the semiconductor surface from corrosion because many photocathodes are relatively stable under such conditions. Some materials are in fact cathodically protected under illumination because they operate in the immunity region of the Pourbaix diagram, while others have extremely slow kinetics for reduction of the surface species and undergo minimal bulk reduction processes. Nevertheless, the use of thin-layer protective coatings can enhance the stability of certain materials; these coatings often eliminate the direct contact between the semiconductor surface and the aqueous electrolyte and therefore increase the complexity of the device structure and fabrication.

Although the introduction of a protection layer generally forms a buried junction, which can lead to Fermi level pinning that is not present at the unprotected photocathode/liquid interface of concern, suitable application of surface layers can also beneficially increase the photovoltage as well as the long-term stability of some photocathode materials.[149] Most of the well-established TCO materials that are used ubiquitously as top contacts in conventional photovoltaic cells and many refractory metal oxides (e.g., TiO_2) are n-type semiconductors, making them suitable to form highly rectifying and photoactive contacts with p-type absorbers (e.g., p-InP or p-Si). Many of these metal oxides are also stable under reducing conditions (e.g., TiO_2; *vide supra*). Thus, several obvious and natural choices often exist for use as surface layers to protect a semiconductor photocathode of interest, when such protection is needed to obtain stable photoreduction behavior.

In certain cases, p-type semiconductors in contact with aqueous electrolytes may spontaneously form protective surface layers. Alternatively, protective layers may form spontaneously when a p-type semiconductor is transiently exposed to oxidizing conditions. Depending on the semiconductor, these surface layers may be insulating, as with Si (SiO_2), or may be n-type conducting, as in the case of InP (In_2O_3). Moreover, the physical and electronic properties (crystallinity, defect density, conductivity, work function, etc.) are likely a function of the conditions under which the layer is formed. Hence, the implementation of a passivation/protection scheme for photocathodes is highly material-specific, and certain materials (particularly Si and InP) have been highly favored for the inherently desirable qualities of their "native" surface coatings under photocathodic conditions. Table 3 summarizes many of the results for hydrogen-evolving photocathode materials that employ surface layers for stabilization and/or improved energy-conversion efficiencies. The content of Table 3 parallels that of

DOI: 10.1021/acs.jpcc.5b05976
J. Phys. Chem. C XXXX, XXX, XXX−XXX

Table 3. Photoelectrosynthetic Systems for Hydrogen Evolution[a]

year	photocathode	protective film composition (thickness, nm)[b]	deposition method	cocatalyst (nm)	electrolyte	solution pH	illumination	reported stability time	stability J (mA cm^{-2})	E(onset) vs RHE (V)	ref
1977	p-Si	TiO_2 (not stated)	CVD	none	0.5 M Na_2SO_4	~7	450 W Xe lamp	"several hours"	<1	−0.14	Kohl[140]
1981	p-InP	"thin surface oxide"	acid etching	Ru, Rh, Pt	1 M HCl with 2 M KCl[c]	0	Sunlight 85 mW cm^{-2}	1 week	–	0.54	Heller and Vadimsky[150]
1982	p-InP	"thin surface oxide"	acid etching	Ru, Rh, Pt	4 M $HClO_4$		100 W QTH, 2−3 suns	24 h	60	0.8	Heller[151]
1988	two-junction nip a-Si	Pt (1.5 nm)	E-beam evaporation	Pt (1.5)	0.5 M H_2SO_4	0	AM1, 100 mW cm^{-2}	–	–	1.6	Sakai[152]
1988	triple-junction a-Si/crystalline-Si	Pt (1.5 nm)	E-beam evaporation	Pt (1.5)	0.5 M H_2SO_4	0	AM1, 100 mW cm^{-2}	–	–	2.0	Sakai[152]
1996	p-Si	(none)		Pt	1 M HCl	0	W halogen 33 mW cm^{-2}	60 d	~ 4	0.3	Maier[153]
1999	p-$GaInP_2$	(none)		Pt	2 M HBr, 2 M $NaClO_4$	~0	W halogen	10 h	35	–	Khasalev[154]
2003	p-Cu_2O	TiO_2 (100)	sputtering	(none)	0.1 M sodium acetate	varied	Xe lamp 70 mW cm^{-2}	–	0.7	0.46	Siripala[155]
2008	p-$CuGaSe_2$	(none)		(none)	0.5 M H_2SO_4	0	natural sunlight	4 h	10	0.1	Marsen[156]
2010	p-$Cu(In,Ga)Se_2$	n-CdS	chemical bath	Pt	0.1 M Na_2SO_4	varied		16 h	9	0.5 at pH 9.5	Yokoyama[157]
2011	p-Si nanopillars	Mo_3S_4	drop cast	Mo_3S_4	1 M $HClO_4$	0	AM1.5G, >635 nm	1 h	9	0.1	Hou[158]
2012	p-Cu_2O nanowires	NiO_x (10)	spin coating	NiO_x	0.1 M Na_2SO_4	6	LED, 425−660 nm, 26 mW cm^{-2}	20 min	0.2	~ 0.5	Lin[159]
2012	p-Cu_2O	AZO/TiO_2 (20/10)	ALD	Pt	0.5 M Na_2SO_4	5	AM1.5G	10 h	1.5	0.4	Paracchino[160]
2012	p-InP, nanotextured	TiO_2 (2−5)	ALD	Ru	1 M $HClO_4$	0	AM1.5	4 h	35	0.73	Lee[161]
2012	n^+p-Si	Ti (9)	sputtering	MoSx	1 M $HClO_4$	0	AM 1.5 >635 nm	1 h	12	0.33	Seger[162]
2012	p-Si	ZnO nanowires	solution growth	Pt	0.25 M Na_2SO_4	7.2	AM1.5	1 h, damage observed	NR	0.2	Sun[163]
2012	n^+p-Si	(none)		Ni−Mo	KHP	4.5	W-halogen 100 mW cm^{-2}	1 h	9.5	0.45	Warren[51]
2012	Cu_2O	AZO (20)/TiO_2 (20)	ALD	Pt	1 M acetate	5	AM1.5	10 h	1	~ 0.3	Paracchino[164]
2013	p-CZTS	AZO/TiO_2	ALD	Pt	0.5 M KP_i	7.0	AM1.5	15 min	0.2	0.3	Rovelli[165]
					0.1 M Na_2SO_4	9.0	AM1.5	15 min	0.3	–	
2013	n^+p-Si	Mo/MoS_2	sputtering/sulfidation	MoS_x	1 M $HClO_4$	0	AM1.5 >635 nm	5 d	10	0.33	Laursen[166]
2013	p-Si	CdS	chemical bath deposition	Pt	0.1 M NaP_i	7	150 W Xe Lamp	12 d	3.5	0.6 (pH 9)	Moriya[167]
2013	$CuInS_2$	C_3N_4	thermal polycondenstation	(none)	0.1 M H_2SO_4	1	Tungsten iodine >400 nm	22 h	0.07	0.36	Yang[168]
2013	n^+p-Si	Ti/TiO_2 (5/100)	sputtering	Pt	1 M $HClO_4$	0	AM1.5 >635 nm	72 h	20	0.51	Seger[169]
2013	nip a-Si	TiO_2 (80)	sputtering	Pt	0.5 M KHP	4	AM1.5G	12 h	11	0.93	Lin[170]
2013	p-Cu_2O	carbon (20)	decomposition of glucose	(none)	1 M Na_2SO_4	~7	AM1.5G	1 h	3	0.6	Zhang[171]
2013	P3HT/PCBM			MoS_3	0.5 M H_2SO_4	~0	Xe lamp >400 nm	45 min	0.05	~ 0.5	Bourgeteau[172]
2013	p-Si MIS	SiO_2 (2)	thermal oxidation	Ti/Pt	0.5 M H_2SO_4	~0	AM1.5	2.5 h	8.13	0.49	Esposito[173]
2014	p-CuO	AZO (20)/TiO_2 (100)	ALD	Pt MoS_{2+x}	0.1 M H_2SO_4	1	AM1.5	2.5 h	8	0.6	Morales-Guio[174]
					0.1 M H_2SO_4	1		5 h	6	0.45	
					0.5 M Na_2SO_4	4		10 h	4.5	0.45	
					0.2 M KHP	9		10 h	2	0.45	
					0.1 M $Na_2B_4O_7$						

DOI: 10.1021/acs.jpcc.5b05976
J. Phys. Chem. C XXXX, XXX, XXX−XXX

Table 3. continued

year	photocathode	protective film composition (thickness, nm)[b]	deposition method	cocatalyst (nm)	electrolyte	solution pH	illumination	reported stability time	stability J (mA cm^{-2})	E(onset) vs RHE (V)	ref
2014	n$^+$p-Si	Mo/MoS_2	sputtering/ sulfidation	MoS_2	0.5 M H_2SO_4	~0	AM1.5	100 h	17	0.35	Benck[175]
2014	p-Cu_2O	AZO (20)/ TiO_2 (100)	ALD	RuO_2	0.5 M Na_2SO_4, 0.1 M NaP_i	5	AM1.5	8 h	5	0.55	Tilley[176]
2014	nanoporous p-Si	Al_2O_3 (2)	ALD	Pt	0.5 M H_2SO_4	~0	AM1.5	12 h	30	< 0	Choi[177]
2014	textured n$^+$p-Si	F:SnO_2/TiO_2	solution deposition	Ir	1 M $HClO_4$	~0	AM1.5	~24 h	3	−0.5	Kast[178]
2014	p-InP	TiO_2 (10)	ALD	Pt	1 M $HClO_4$	~0	AM1.5	2 h	24	0.80	Lin[179]
2014	p-Si	Ti/Ni	E-beam evaporation	Ni	1 M KOH KB_i	14	150 W Xe lamp	12 h	10	0.3	Feng[180]
						~9.5		12 h		0.25	
2015	multicrystalline n$^+$p-Si	Al_2O_3 (4.5)	ALD	Pt	0.5 M K_2SO_4 + 0.5 M H_2SO_4	~0	AM1.5	100 h	27	−0.2–0	Fan[181]
2015	p-Si	$SrTiO_3$	MBE	Pt	0.5 M H_2SO_4	~0	AM1.5	35 h	30	0.45	Ji[182]

[a]Illumination is simulated AM1.5G unless noted. Table is for photocathodes that evolve H_2 and for which the stability time is reported. [b]Outermost layer is the final layer listed, and layer closest to the semiconductor is the first layer listed. [c]Cl_2 produced at counter-electrode.

Table 1, with the exception that the onset potential is reported directly relative to the RHE potential in the electrolyte of interest. Additionally, the following sections discuss stabilization of hydrogen-evolving photocathodes. They are organized by absorber composition, rather than protective layer composition, beginning with Si, continuing with III−V materials, and concluding with other semiconducting photocathodes. This organization deviates from the corresponding section on photoanodes (Section 3) because the formation of conductive oxides and cathodic protection make photocathode stability and performance highly dependent on the absorber.

4.2. Protection of p-Si Photocathodes. According to early Pourbaix diagrams,[26] p-Si is not thermodynamically stable under aqueous conditions. However, a recently revised Si Pourbiax diagram[32] shows a region of stability under cathodic potentials. In alkaline media, Si rapidly oxidizes and dissolves via chemical etching, and the dissolution cannot be entirely arrested by electrochemical means. However, under neutral to acidic conditions, Si forms a passivating oxide that is stable toward dissolution, although the oxide can present a barrier to electron transfer. Thus, surface coatings can stabilize the HER performance of p-Si photocathodes by facilitating interfacial electron transfer and/or by preventing the formation of insulating Si oxides. Under negative applied potentials in acid, Si cannot be further reduced or corroded, but a layer of silicon oxide may be formed in the dark under resting conditions. In the following, we describe some examples of protection strategies developed for p-Si photocathodes.

Since Si does not corrode appreciably under acidic conditions many groups have focused on the development of Si photocathodes with metallic cocatalysts to facilitate hydrogen evolution. Precious metal catalysts are widely used for improving the energy-conversion efficiency of Si photocathodes. These catalysts can reduce activation barriers for the HER and also directly mediate electron transfer from the Si absorber to the electrolyte, which mitigates the effects of the passivating oxide that can form under aqueous conditions on the bare Si surface. Work in the early 1980s on Si photocathodes showed that silicon coated with electrodeposited layers of noble metals could facilitate electrochemical hydrogen evolution in an energy-producing fashion.[183] Around the same time, Heller and co-workers studied the performance and stability of Pt coated p-Si photocathodes.[184] In 1996, Maier et al. elaborated on these results through careful control of catalyst deposition conditions and thicknesses and explored the activity and stability of such systems under a variety of conditions.[153] An optimal thickness of Pt deposited electrochemically produced a buried Schottky junction to p-Si via silicide formation, facilitating charge separation. Onset potentials in the range of 300−500 mV vs RHE were observed, with larger photovoltages observed at higher pH (Figure 9), and the photocathodes were stable for 60 days of continuous operation under illumination in 1 M HCl(aq).

"Black silicon," formed by metal-catalyzed electroless etching, has been reported to provide improved optical absorption compared to planar Si control samples. However, without a catalyst, the onset potential for cathodic photocurrent is still >100 mV negative of 0 V vs RHE.[185] Use of a Pt cocatalyst shifts the onset to 400 mV vs RHE but leads to a reduction in photocurrent density to 18 mA·cm^{-2} consistent with parasitic light absorption by the Pt.[186] Direct Pt deposition via ALD has been performed on p-Si microwires, but the onset potentials are smaller than those observed for Pt deposited onto radial p-n$^+$ Si

DOI: 10.1021/acs.jpcc.5b05976
J. Phys. Chem. C XXXX, XXX, XXX−XXX

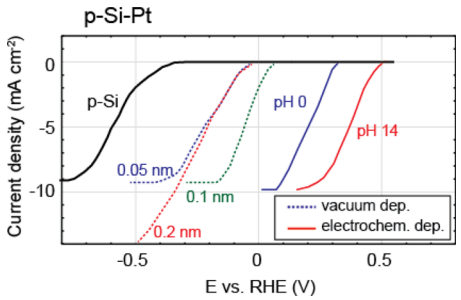

Figure 9. CV data from p-Si photocathodes with thin Pt layers. Illumination intensity is approximately 0.3 suns. Adapted from Maier, C.U.; Specht, M.; Bilger, G. Hydrogen evolution on platinum-coated p-silicon photocathodes. *Int. J. Hydrogen Energy* **1996**, *21* (10), 859 with permission from Elsevier.[153]

microwire arrays.[187,188] Warren et al. formed a buried radial p-n$^+$ junction in Si microwires and reported a 500 mV vs RHE onset for H_2 production using an earth-abundant Ni−Mo HER catalyst.[51] However, non-noble metal alloys such as Ni−Mo chemically corrode under acidic conditions, limiting the stability of these photocathodes.[189] Recent attempts to mitigate such corrosion have focused on the integration of acid-stable CoP electrocatalysts into n$^+$-p Si microwire arrays, yielding an onset potential of 0.45 V vs RHE and 12 h of stability under simulated 100 mW cm^{-2} illumination.[52]

MoS_2 has been used as an integrated HER catalyst on Si microwires[158] and on planar p-n$^+$ electrodes.[166,175] MoS_2 is a particularly interesting catalyst because it is anticipated to be less costly than noble-metal catalysts, and it is very stable under acidic conditions. Multiday stability has been reported for p-Si coated with MoS_2, but the onset potential of 200 mV vs RHE and light-limited current densities of 10 mA cm^{-2} are both less than the values typically observed with p-n$^+$ Si device structures in conjunction with precious metal HER catalysts.

In 1977, Bard and co-workers[140] coated p-Si (and p-GaAs, see below) with TiO_2 grown by CVD. However, only small cathodic photocurrents were observed, and the behavior was attributed to adverse band bending at the oxide/semiconductor interface forming a barrier for electrons to cross the solid/solid interface. Recently, conducting oxides have been used on p-Si photocathodes. One common strategy is to use a photovoltaic p-n$^+$ junction that contains a TCO overlayer. Seger et al. used this approach and found that a 5 nm metallic Ti followed by a thick (>100 nm) layer of TiO_2 and a Pt cocatalyst on top of a Si p-n$^+$ homojunction allowed operation of the electrically isolated photovoltaic buried junction device for several weeks of continuous operation for the HER in 1 M $HClO_4$(aq).[169] A 520 mV onset potential vs RHE was observed, which is consistent with the use of a buried n$^+$-p Si homojunction. Similar results in terms of onset potential (510 mV vs RHE) and stability were obtained using ALD-deposited TiO_2.[190] This work shows that TiO_2 can facilitate transfer of electrons through conduction-band states. Hupp and co-workers also observed that TiO_2 allows for facile electron conduction that is largely independent of the thickness of protective coatings.[191]

Other oxides have been explored as coatings on p-type Si. Choi and co-workers used ALD-grown Al_2O_3 to coat p-Si.[177] The onset potential was negative of 0 V vs RHE, meaning hydrogen was not evolved in an energy-producing fashion. Sun et al. reported the use of planar and nanostructured n-ZnO overlayers on p-Si photocathodes.[163] Photocathodic currents were observed with onset potentials near 0 V vs RHE, although significant degradation in performance was observed after 1 h of operation. A thin film of $SrTiO_3$ was recently epitaxially grown directly on Si(001) by molecular-beam epitaxy and then patterned with islands of metal HER catalysts. A maximum photocurrent density of 35 mA cm^{-2}, an open-circuit voltage of 450 mV, and stable performance for 35 h was observed in 0.5 M H_2SO_4.[182] Spray-pyrolysis-deposited F:SnO_2/TiO_2 overlayers have been integrated into p-n$^+$ Si-based photovoltaics, with ideal regenerative cell efficiencies of up to 10.9% albeit with substantial degradation in performance after 80 h of operation in 1 M KOH(aq).[178]

In an approach that combines aspects of oxide passivation and HER catalyst integration, Esposito et al.[173] formed a p-Si/SiO_2/bilayer metal (metal−insulator−semiconductor, MIS) with a tunneling oxide. An underlayer of Ti was used to induce a rectifying barrier to the p-Si, and an overlayer of Pt was used as the HER catalyst. An onset potential of 490 mV vs RHE was observed, although the observed fill factors were low. The photocathodes were stable for at least 2.5 h under galvanostatic conditions at 8 mA cm^{-2}. Feng et al. also used a Ti underlayer to obtain a rectifying junction to p-Si photocathodes. Upon deposition of a thin (5 nm) overlayer of Ni, these researchers observed onset potentials ranging from 250 to 300 mV in pH 9.5 potassium borate (KBi) buffer and 1 M KOH(aq), respectively. 12 h stability tests suggested that the Ti underlayer did not protect the underlying Si in the strongly alkaline electrolyte, but greater stability was observed in the mildly alkaline borate buffer solution.[180]

Amorphous silicon has been investigated extensively as a light-absorbing component in solar-driven water splitting. A number of demonstrations of overall solar water splitting have used triple-junction amorphous Si solar cell stacks in combination with HER and OER catalysts.[78,192] Often in these designs the a-Si surface is isolated from the electrolyte by a thick TCO layer or by a metal. Toor et al.[193] showed that micropixelation of a-Si photocathodes into 100 μm square areas isolated with SiN_x could double the lifetime under HER conditions in buffered pH 10 aqueous media. Lin et al.[170] demonstrated 12 h stability of an a-Si p-i-n structure via a 100 nm sputtered TiO_2 layer and either Pt or Ni−Mo catalysts. Notably, onset potentials up to 930 mV vs RHE were observed for these amorphous-Si-based, single junction photocathodes under 1 Sun illumination. Sakai et al. reported that a 1.5 nm Pt layer can enable tandem-junction amorphous Si or triple-junction amorphous Si/crystalline Si tandem PV-biased PEC photocathodes to operate in 0.5 M H_2SO_4(aq).[152] The reported photocurrent densities were 2.5−3 mA cm^{-2}, partly due to the opacity of Pt overlayers. Yamada et al. also reported a two-junction n-i-p amorphous Si PV electrolysis cell that was fabricated in an inverted supercell setup (dark cathode) with the back sides protected by stainless sheets coated with a CoMo HER catalyst; in this configuration, 18 h of operation were reported at pH 13.[194]

The Texas Instruments (TI) Corporation performed extensive work to protect Si light absorbers as part of their development of an HBr electrolysis device based on a serial connection of two Si p-n microspherical junctions.[195−197] Notably, the TI researchers deposited noble metal catalysts for hydrogen evolution directly on the surface of the Si absorber homojunctions, and a glass matrix protected the uncoated Si surfaces from direct contact. Thus, the only surfaces in direct contact with the electrolyte were the catalyst or the glass. The

DOI: 10.1021/acs.jpcc.5b05976
J. Phys. Chem. C XXXX, XXX, XXX−XXX

long-term stability of the associated noble metal catalysts was assessed in detail, and the greatest source of corrosion was residual instability of the photocathode catalyst material under nonoperating (i.e., dark) conditions rather than the underlying semiconductor absorber layer.[198]

4.3. Protection of III−V Photocathodes. Like Si, most III−V materials (e.g., GaAs, GaP, InP) oxidize readily under aqueous conditions. However, the stability and electronic properties of the resulting oxides vary greatly with the composition of the semiconductor. In addition, at negative potentials, group III elements can be further reduced to their metallic form.[199] For example, metallic Ga or In can be formed from GaAs, GaP, or InP.

Heller et al. investigated p-InP photocathodes for the HER in the early 1980s.[151,200,201] Onset potentials of >600 mV vs RHE and current densities of 25 mA cm^{-2} under 80 mW cm^{-2} simulated illumination were measured. The InP needed to be operated intermittently under anodic conditions to regrow a thin oxide layer that was presumed to be critical to the observed performance.[200] Work by Lewerenz and co-workers has clarified this picture[202] and has also delineated the types of surface oxides that are produced *in situ* in contact with different electrolytes.[203] Lee et al. found that high surface area InP structures formed by reactive ion etching (RIE) with 2−5 nm of ALD-deposited TiO_2 performed very well for hydrogen evolution. Photocurrent onset potentials of >600 mV vs RHE, current densities of 37 mA cm^{-2} under 100 mW cm^{-2} of simulated solar illumination, and ideal regenerative cell conversion efficiencies of over 13% were observed.[161] The favorable onset potential was attributed to the formation of a p-InP/n-InO_x heterojunction, which was further stabilized by the ALD-grown TiO_2. The structured InP photoelectrodes showed negligible degradation over 4 h of operation, which the authors attributed to the TiO_2 coating as well as favorable bubble-release properties of the structured surface. Lin et al. subsequently increased the onset potential for InP/TiO_2 photocathodes to over 800 mV vs RHE by manipulation of the chemistry at the semiconductor−oxide interface.[179]

Other III−V semiconductor photocathodes have not exhibited performance or stability comparable to that observed for p-InP-based HER systems. Early work by Bard and co-workers attempted to protect p-GaAs with TiO_2 grown by CVD. As in their parallel efforts with silicon, only small cathodic photocurrents were observed, which was attributed to unfavorable interfacial energetics.[140] In the case of GaP photocathodes, neither the growth of GaO_x layers nor the integration of a Pt HER catalyst yielded improvements in the hydrogen production behavior, and the onset potentials were <0.4 V vs RHE.[199] H_2 and O_2 have been produced from water without an external bias using a multijunction photovoltaic absorber that used a p-GaInP top layer in direct contact with an aqueous electrolyte.[204] H_2 was directly evolved at the photocathode, and O_2 was evolved at the dark anode of the cell which contained 1 M H_2SO_4 as the electrolyte. The lifetime of this cell was limited by photocorrosion of the GaInP layer exposed to the acidic electrolyte.[205,206] A long-term passivation strategy for this material has not yet been demonstrated, although nitridation by ion bombardment was found to markedly improve the stability of GaP-based absorbers.[207]

Similar to the Texas Instruments work on HBr electrolysis using Si absorbers, Khaselev and Turner reported the net electrolysis of HI and HBr using a multijunction photoelectrode consisting of a GaAs photovoltaic connected to a p-GaInP overlayer through a tunnel junction. Using noble metal cocatalysts, the electrode assembly facilitated efficient unassisted hydrogen halide splitting for 8−10 h even under optical concentration.[154]

4.4. Protection of Other Photocathodes. The chemical stability of several photocathodes other than Si and III−V materials has also been investigated. Cu_2O is an interesting candidate for protection strategies because Cu_2O is thermodynamically unstable under HER conditions and forms metallic Cu at the surface under illumination. Siripala et al. reported that a Cu_2O/TiO_2 heterojunction structure, with the Cu_2O grown electrochemically and the TiO_2 grown by electron-beam evaporation and without explicit addition of a HER cocatalyst, was active and stable as a photocathode.[155] This system has also been investigated recently by Grätzel and co-workers. A bilayer AZO (Al-doped ZnO)/TiO_2 surface coating grown by ALD produced an onset potential of 0.4 V vs RHE. The use of Pt as a cocatalyst yielded photocurrent densities of ∼8 mA cm^{-2} at 0 V vs RHE.[160] The degradation over time was stated to be due to deactivation of the Pt catalyst as opposed to corrosion of the Cu_2O.[164] RuO_2 appears to have a longer lifetime as an HER catalyst in this photocathode configuration, and subsequent work has reported half cell efficiencies of up to 6% with 96 h of continuous operation using a p-Cu_2O/AZO/TiO_2/RuO_x structure.[176]

Cu_2O nanowires have also been protected during operation for the HER. Lin et al. reported that Cu_2O nanowires grown by a chemical-bath method could be stabilized by deposition of spin-coated NiO.[159] Onset potentials >0.4 V vs RHE were reported but with relatively low light-limited current densities (∼1 mA cm^{-2}) and a Faradaic efficiency of 33%. p-CuO/ZnO nanowire heterostructures have also been used to generate H_2, although at lower efficiency than has been obtained using Cu_2O-based structures.[208]

P-type absorbers that are used in thin-film solar cells are also being investigated as photocathodes for solar-driven water splitting. Marsen et al. reported that p-$CuGaSe_2$ photocathodes produced photocurrent densities of up to 10 mA cm^{-2} under 1 sun illumination with no cocatalyst at pH 0.3, with 4 h of stability.[156] Domen and co-workers have employed a heterojunction approach using an n-CdS emitter, similar to the solar cell configuration for a p-$CuGaSe_2$ and p-Cu(In,Ga)-Se_2 (CIGS) absorbers.[157,167] With a Pt cocatalyst, stable photocurrents were observed for up to 10 days, with an onset potential of 0.7 V vs RHE. Modification of porous p-type $CuInS_2$ films with thin layers of Pt/TiO_2/CdS significantly increased the cathodic photocurrent and onset potential through the formation of a p−n junction on the surface, whereas when the electrode was instead only modified with Pt/CdS, the photoelectrode decayed rapidly due to the photocorrosion of CdS.[209] The use of Pt/In_2S_3 produced a similar enhancement effect on $CuInS_2$.[210] The effective protection by sulfide for these type of materials indicates the importance of interfacial structure and band alignment. Jacobsson et al. investigated CIGS/CdS/ZnO/Pt heterostructures and observed modest photocurrents. Onset potentials positive of 0 V vs RHE were produced by isolating the solar cell and using a Pt electrode.[211] Rovelli et al. examined a CuZnSnS (CZTS)/AZO/TiO_2 structure, similar to the configuration discussed above for Cu_2O.[165] The protected structure exhibited an onset potential of 360 mV vs RHE, 150 mV higher than an uncoated control sample, with 22 h of stability under acidic conditions. A C_3N_4 film made by thermal polycondensation has been

DOI: 10.1021/acs.jpcc.5b05976
J. Phys. Chem. C XXXX, XXX, XXX−XXX

reported to act as a protective layer on $CuInS_2$. C_3N_4 is a polymeric semiconductor with a bandgap of about 2.7 eV, which has shown to be photocatalytically active for H_2 evolution.[212] The $C_3N_4/CuInS_2$ composite photocathode material generated a cathodic photocurrent at potentials up to +0.36 V vs RHE in 0.1 M H_2SO_4(aq), which corresponds to a 150 mV more positive onset potential of cathodic photocurrent than was observed for unmodified $CuInS_2$ semiconducting thin-film photocathodes. However, the photocurrent was diminished compared to $CuInS_2$ without the C_3N_4.[168]

4.5. Summary and Perspective of Photocathode Protection. For most of the photocathode materials discussed above, a structure consisting of a p-type absorbing layer, in conjunction with either a homojunction or heterojunction to provide an electron-selective contact, a conducting oxide layer, and an optically thin HER catalyst, produces good performance in terms of onset potential, current density, and stability.[51,151,161,164,169,200] In the related field of solar photovoltaics, it is increasingly being recognized that reducing carrier recombination through minority-carrier selective interfaces is critical for obtaining the maximum efficiency from a given absorber material.[213] In the case of Si, this has led to development of thin oxide or larger band gap layers that enable minority-carrier conduction but also electronically separate the contact metal from the Si.[214,215] This approach can lead to substantial reductions in surface recombination and concomitant increases in open-circuit voltages. Given that many of the entries in Table 3 are for a semiconductor−oxide−metal combination, significant opportunities remain to optimize the oxide not only for corrosion protection but also for reduction of interfacial recombination.[179] These strategies can continue to be leveraged to stabilize photocathode materials having band gaps in the 1.1−1.7 eV range and to further improve the energy-conversion efficiency and stability of such materials, particularly using well-established light absorbers such as Si and thin-film chalcogenides. Further improvements in efficiency and stability should also be possible through functional improvements, e.g., lowering catalyst overpotentials or engineering of light-trapping surfaces.

5. OVERALL OUTLOOK AND CONCLUSIONS

Chemical stability and protection are critically important in informing many aspects of solar-fuel systems, including device geometry, semiconductor/liquid junction performance, management of ion transport, and eventually manufacturing and system cost. Protective films can enable the use of technologically important, nonoxide photovoltaic materials in environments containing liquid electrolytes, for not only water splitting but also for photochemical processes such as hydrogen−halide electrolysis and electrochemical reduction of CO_2 to make commodity chemicals. This strategy also may enable the use of particle-based light absorbers for fuel production and environmental remediation. Development of protection strategies involving thin surface films has become a highly active research field since ca. 2011, and it is being pursued in tandem with the development of stable oxide semiconductor absorbers that have appropriate electronic properties and that might not require protective layers to exhibit oxidative stability in solar-driven water splitting (e.g., Fe_2O_3, $BiVO_3$).

As is readily apparent from Tables 1−3, enormous progress in the development of protective films has been made by recent research efforts. Of all of the protective film compositions, titanium oxide has emerged as a promising material for protection of both photocathodes and photoanodes. TiO_2 is highly stable and transparent, and appropriate conduction pathways are available for electrons via the conduction band (for photocathodes) and, in some cases, for holes via apparent in-gap defect states (for photoanodes). The development and study of TiO_2 and similar oxides for protection will likely involve further study/development of the band and defect transport in these materials, as well the interfacial electronic properties of TiO_2 with the nonoxide semiconductors. In the case of buried PV junctions, the interfacial electronic properties may be less important for functionality than in true PEC junctions, but the use of buried junctions increases the complexity and therefore the cost of the resulting devices. Thus, continued work on protection strategies for both PV and PEC systems is certainly warranted. In the following, we conclude with several recommendations for future directions and outlook for this research area.

5.1. Demonstration Guidelines. Consistent experimental assessment of stability would aid in comparing the relative performance of different protective strategies. Guidelines have been suggested,[216,217] but a few key aspects are noted here. Specifically, the current density utilized for long-term stability experiments should be near what would be expected under operation for a potential device (between 10 and 20 mA cm^{-2} and at, or near, the anticipated operating potential or maximum power point). Further, reference to RHE in addition to the employed reference electrode (if not RHE) greatly aids in rapid comparisons between studies. Measurement of the Faradaic efficiency of O_2 and H_2 gas evolution is also recommended to distinguish fuel formation from electrochemical corrosion.[216] Studies that assess decomposition products in the electrolyte solution[98,218] and/or that determine quantitatively the extent of mass loss of the electrode,[95] as opposed to simple monitoring of the photocurrent, can provide important insight into the relative faradaic yields of photoelectrosynthetic reactions vs corrosion of the electrodes. Standards reported by the U.S. Department of Energy indicate goals of stable PEC operation of 5000 h by 2018 and recommend a minimum of 200 h for laboratory demonstrations.[219] The long-term stability of the other electrochemical components (frits, reference electrodes) must be carefully considered for long-term experiments especially because many studies involve strongly alkaline electrolytes, which slowly etch glass components. Key figures of merit to be measured are the voltage at maximum power point and the length of time that the photoelectrode can operate at this maximum power point.

5.2. Protected Photoelectrodes vs Buried Junctions with Protection. The use of buried junctions from photovoltaic devices, with subsequent protection, is both conceptually and practically different from the use of photoelectrodes that do not contain a buried PV junction prior to protection. First, the processing to form buried junctions in photovoltaic devices is more complicated than the simple growth of the light absorber itself. For some materials, no processes have been developed to form high figure of merit p−n or heterojunction formation (e.g., Cu_2O). Once the buried junction is formed, e.g., in planar np^+-Si solar cells, the resulting device can be readily wired to an electrolyzer or to a membrane-electrode-assembly device, instead of being protected and used as a "cosmetically integrated" PEC device. In some cases, formation of electrical contacts is very difficult in practice, such as with

DOI: 10.1021/acs.jpcc.5b05976
J. Phys. Chem. C XXXX, XXX, XXX−XXX

arrays of Si microwires,[220] even if buried junctions are already formed. In this case, the wire morphology is beneficial for making PEC devices instead of PV devices since the liquid contact is inherently conformal. Further, diffusion doping of polycrystalline materials can be highly detrimental to grain boundaries (e.g., majority carrier shunting) and represents another possible advantage of the PEC-based junction. The option of protecting photoelectrodes without forming buried junctions is thus preferred to making a buried junction, provided high figure-of-merit junctions can be produced. In fact, there have been ample examples for high performance in polycrystalline PEC devices.[18]

5.3. Performance Comparisons. Materials systems such as crystalline-Si, amorphous-Si, III−Vs (GaAs, GaP, and InP), II−VIs (CdTe and CdSe), and CIGS can form high-quality p−n homojunctions or heterjunctions, so high photovoltages can be obtained from protected photoelectrodes. Materials systems like $BaTaO_2N$, $BiVO_4$, and Ta_3N_5 have not been demonstrated to produce high photovoltages in homojunction, heterojunction, or aqueous liquid-junction systems. We note that low minority-carrier diffusion lengths and other recombination pathways could also be responsible for the low V_{oc} values for the PEC junctions studied. Furthermore, materials like Si can form buried metal−semiconductor (MS) or metal−insulator−semiconductor (MIS) junctions with thin-metal layer protection, and their performance should be characteristic of the solid-state junction that is formed. Hence, the various possible device configurations involved in photoelectrode stabilization should be considered when evaluating the performance of the different types of system. For example, 600 mV V_{oc} is routine for a buried Si homojunction and has been reported repeatedly for various protection strategies with np^+-Si or pn^+-Si junctions, whereas 550 mV would be an excellent photovoltage for a protection layer on only a Si absorber. Alternatively, no Si-based MS junctions have been demonstrated to produce such high a photovoltage, but 550 mV photovoltages from an Ir/TiO_2/n-Si MIS structure[119] constitute excellent performance from such systems.

5.4. Performance Enhancement. Enhancement of performance may take the form of increases in the photoelectrosynthetic figures of merit (e.g., photovoltage, photocurrent) as well as increases in longevity/robustness of the electrodes. In the case of PV junctions, the protective film must simply allow for light transmission and electron/hole transmission (i.e., not present a resistive barrier). However, in the PEC case, favorable band bending and carrier selectivity must be present with the protective film to establish the requisite charge-transfer asymmetry. PEC or adaptive[61,62] junctions warrant detailed investigation both theoretically and experimentally because the interfacial structure/chemistry and the catalyst properties can largely dictate the overall photoelectrosynthetic behavior.

5.5. New Directions. Several productive activities may advance photoelectrode stability beyond the current state-of-the-art. For example, several classes of prospective protection materials have not been thoroughly explored, such as metal carbides, metal nitrides, and 2-dimensional (2-D) materials. Metal carbides and nitrides are often known for their mechanical hardness, as well as their chemical stability. The explosion of interest in 2-D materials, such as graphene, MoS_2, and hexagonal boron nitride (h-BN), may provide a wide variety of compositions to examine for use in conjunction with semiconducting electrodes. Indeed, MoS_2 films have already been used in a predominantly catalytic role for hydrogen-evolving photocathodes. The study of 2-D materials for stabilization of semiconductor electrodes may yield valuable information about the interaction between these materials, such as how junctions form, based on the electronic and electrochemical properties of the 2-D layers.[221] On the basis of these and other new directions, development of novel materials and understanding of the physical processes and corrosion behavior of semiconductor electrodes is needed to enable robust semiconductor-based solar fuel generators.

AUTHOR INFORMATION

Corresponding Authors

*E-mail: nslewis@caltech.edu.

*E-mail: strand@lehigh.edu. Phone: 1 (610) 758-4197.

Notes

The authors declare no competing financial interest.

Biographies

Dr. Shu Hu is a senior postdoctoral scholar at Joint Center for Artificial Photosynthesis. He received his B. Eng. (Honors) from Tsinghua University in 2006 and then completed a Ph.D. in Materials Science at Stanford University in 2011. Shu then joined the group of Prof. Nathan S. Lewis in Division of Chemistry and Chemical Engineering at California Institute of Technology, where his work spans experimental and modeling areas in Si and III−V nanocrystal synthesis, nanophotonic phenomena, and solid−electrolyte interfaces for photoelectrochemical solar-fuel production. His main thrust includes the stabilization of technologically important, efficient, yet unstable semiconductors under photoanodic conditions relevant to water oxidation.

Dr. Nathan S. Lewis is the George L. Argyros Professor of Chemistry at the California Institute of Technology and the Scientific Director of the Joint Center for Artificial Photosynthesis, the DOE's Energy

DOI: 10.1021/acs.jpcc.5b05976
J. Phys. Chem. C XXXX, XXX, XXX−XXX

Innovation Hub in Fuels from Sunlight. Professor Lewis is Principal Investigator of the Beckman Institute Molecular Materials Resource Center. His research interests include artificial photosynthesis and electronic noses. Nate continues to study ways to harness sunlight and generate chemical fuel by splitting water to generate hydrogen. He is developing the electronic nose, which consists of chemically sensitive conducting polymer film capable of detecting and quantifying a broad variety of analytes. Technical details focus on light-induced electron transfer reactions, both at surfaces and in transition metal complexes, surface chemistry and photochemistry of semiconductor/liquid interfaces, novel uses of conducting organic polymers and polymer/conductor composites, and development of sensor arrays that use pattern recognition algorithms to identify odorants, mimicking the mammalian olfaction process.

Joel W. Ager, III is a Staff Scientist in the Materials Sciences Division of Lawrence Berkeley National Laboratory and an Adjunct Professor in the Materials Science and Engineering Department, UC Berkeley. He is a Project Leader in the Joint Center for Artificial Photosynthesis (JCAP) and a Principal Investigator in the Electronic Materials Program and in the Singapore Berkeley Initiative for Sustainable Energy (SinBeRISE). He graduated from Harvard College in 1982 with an A.B. in Chemistry and from the University of Colorado in 1986 with a Ph.D. in Chemical Physics. After a postdoctoral fellowship at the University of Heidelberg, he joined Lawrence Berkeley National Laboratory in 1989. His research interests include the fundamental electronic and transport characteristics of photovoltaic materials, development of new photoanodes and photocathodes based on abundant elements for solar fuel production, and the development of new oxide and sulfide based transparent conductors.

Dr. Jinhui Yang received her Ph.D. degree from Dalian Institute of Chemical Physics (DICP), Chinese Academy of Sciences (CAS). She is currently postdoctoral researcher at Joint Center for Artificial Photosynthesis (JCAP), Lawrence Berkeley National Laboratory (LBNL). Her research interests include corrosion protection and interface engineering for solar energy conversion.

Dr. James McKone received a BA in Chemistry and Music from Saint Olaf College in 2008 and a Ph.D. in chemistry from the California Institute of Technology in 2013, where he developed materials and methods for solar-driven water splitting with Harry Gray and Nate Lewis. Currently a postdoctoral researcher at Cornell University, James has studied materials for solar energy conversion and large-scale batteries with Héctor Abruña and Francis DiSalvo. His current research continues to focus on fundamental and applied studies of electrochemical energy conversion and storage.

Professor Nicholas Strandwitz completed his B.S. in Engineering Science at The Pennsylvania State University in 2004. He earned his Ph.D. from the Materials Department at University of California Santa Barbara with Professor Galen D. Stucky. After conducting postdoctoral work at California Institute of Technology working with Professor Nathan S. Lewis he joined the Materials Science and Engineering Department at Lehigh University in 2013. Dr. Strandwitz' current research interests include new methods and chemistries in atomic layer deposition and interfacial electronic properties of semiconductor surfaces and interfaces.

■ ACKNOWLEDGMENTS

NCS acknowledges start-up funds from Lehigh University. JRM acknowledges a postdoctoral research award from the U.S. Department of Energy, Office of Energy Efficiency and Renewable Energy through the SunShot Initiative. SH, NSL, JWA, and JY were supported by the Joint Center for Artificial Photosynthesis, a DOE Energy Innovation Hub, supported through the Office of Science of the U.S. Department of Energy under Award Number DE-SC0004993, and NSL was also supported by the National Science Foundation under Award Number CHE-1214152, the Department of Energy, Office of

DOI: 10.1021/acs.jpcc.5b05976
J. Phys. Chem. C XXXX, XXX, XXX−XXX

Basic Energy Sciences under Award Number DE-FG02-03ER15483, and the Gordon and Betty Moore Foundation under Award Number GBMF1225.

REFERENCES

(1) Smil, V. In *Energy in Nature and Society: General Energetics of Complex Systems*; MIT Press: Cambridge, MA, 2008; p 496.

(2) Walter, M. G.; Warren, E. L.; McKone, J. R.; Boettcher, S. W.; Mi, Q.; Santori, E. A.; Lewis, N. S. Solar Water Splitting Cells. *Chem. Rev.* **2010**, *110*, 6446−6473.

(3) Gray, H. B. Powering the Planet with Solar Fuel. *Nat. Chem.* **2009**, *1*, 7−7.

(4) Turner, J. A. A Nickel Finish Protects Silicon Photoanodes for Water Splitting. *Science* **2013**, *342*, 811−812.

(5) Lewis, N. S.; Nocera, D. G. Powering the Planet: Chemical Challenges in Solar Energy Utilization. *Proc. Natl. Acad. Sci. U. S. A.* **2006**, *103*, 15729−15735.

(6) Ronge, J.; Bosserez, T.; Martel, D.; Nervi, C.; Boarino, L.; Taulelle, F.; Decher, G.; Bordiga, S.; Martens, J. A. Monolithic Cells for Solar Fuels. *Chem. Soc. Rev.* **2014**, *43*, 7963−7981.

(7) Turner, J. A. Sustainable Hydrogen Production. *Science* **2004**, *305*, 972−974.

(8) Brillet, J.; Cornuz, M.; Formal, F. L.; Yum, J.; Grätzel, M.; Sivula, K. Examining Architectures of Photoanode−photovoltaic Tandem Cells for Solar Water Splitting. *J. Mater. Res.* **2010**, *25*, 17−24.

(9) Prevot, M. S.; Sivula, K. Photoelectrochemical Tandem Cells for Solar Water Splitting. *J. Phys. Chem. C* **2013**, *117*, 17879−17893.

(10) Nielander, A. C.; Shaner, M. R.; Papadantonakis, K. M.; Francis, S. A.; Lewis, N. S. A Taxonomy for Solar Fuels Generators. *Energy Environ. Sci.* **2015**, *8*, 16−25.

(11) Ager, J. W., III; Shaner, M.; Walczak, K.; Sharp, I. D.; Ardo, S. Experimental Demonstrations of Spontaneous, Solar-Driven Photoelectrochemical Water Splitting. *Energy Environ. Sci.* **2015**, DOI: 10.1039/C5EE00457H.

(12) Bak, T.; Nowotny, J.; Rekas, M.; Sorrell, C. C. Photo-Electrochemical Hydrogen Generation from Water using Solar Energy. Materials-Related Aspects. *Int. J. Hydrogen Energy* **2002**, *27*, 991−1022.

(13) Bolton, J. R.; Strickler, S. J.; Connolly, J. S. Limiting and Realizable Efficiencies of Solar Photolysis of Water. *Nature* **1985**, *316*, 495−500.

(14) Weber, M. F.; Dignam, M. J. Efficiency of Splitting Water with Semiconducting Photoelectrodes. *J. Electrochem. Soc.* **1984**, *131*, 1258−1265.

(15) Hu, S.; Xiang, C.; Haussener, S.; Berger, A. D.; Lewis, N. S. An Analysis of the Optimal Band Gaps of Light Absorbers in Integrated Tandem Photoelectrochemical Water-Splitting Systems. *Energy Environ. Sci.* **2013**, *6*, 2984−2993.

(16) Doscher, H.; Geisz, J. F.; Deutsch, T. G.; Turner, J. A. Sunlight Absorption in Water - Efficiency and Design Implications for Photoelectrochemical Devices. *Energy Environ. Sci.* **2014**, *7*, 2951−2956.

(17) Seitz, L. C.; Chen, Z.; Forman, A. J.; Pinaud, B. A.; Benck, J. D.; Jaramillo, T. F. Modeling Practical Performance Limits of Photoelectrochemical Water Splitting Based on the Current State of Materials Research. *ChemSusChem* **2014**, *7*, 1372−1385.

(18) Coridan, R. H.; Nielander, A. C.; Francis, S. A.; McDowell, M. T.; Dix, V.; Chatman, S. M.; Lewis, N. Methods for Comparing the Performance of Energy-Conversion Systems for use in Solar Fuels and Solar Electricity Generation. *Energy Environ. Sci.* **2015**, DOI: 10.1039/C5EE00777A.

(19) Hernandez-Pagan, E.; Vargas-Barbosa, N.; Wang, T.; Zhao, Y.; Smotkin, E. S.; Mallouk, T. E. Resistance and Polarization Losses in Aqueous Buffer-Membrane Electrolytes for Water-Splitting Photoelectrochemical Cells. *Energy Environ. Sci.* **2012**, *5*, 7582−7589.

(20) Jin, J.; Walczak, K.; Singh, M. R.; Karp, C.; Lewis, N. S.; Xiang, C. An Experimental and Modeling/Simulation-Based Evaluation of the Efficiency and Operational Performance Characteristics of an Integrated, Membrane-Free, Neutral pH Solar-Driven Water-Splitting System. *Energy Environ. Sci.* **2014**, *7*, 3371.

(21) McKone, J. R.; Lewis, N. S.; Gray, H. B. Will Solar-Driven Water-Splitting Devices See the Light of Day? *Chem. Mater.* **2014**, *26*, 407−414.

(22) Sun, K.; Shen, S.; Liang, Y.; Burrows, P. E.; Mao, S. S.; Wang, D. Enabling Silicon for Solar-Fuel Production. *Chem. Rev.* **2014**, *114*, 8662.

(23) Liu, R.; Zheng, Z.; Spurgeon, J.; Yang, X. Enhanced Photoelectrochemical Water-Splitting Performance of Semiconductors by Surface Passivation Layers. *Energy Environ. Sci.* **2014**, *7*, 2504−2517.

(24) Pourbaix, M. In *Lectures on Electrochemical Corrosion*; Plenum Press: New York-London, 1973.

(25) Acevedo-Peña, P.; Vazquez-Arenas, J.; Cabrera-Sierra, R.; Lartundo-Rojas, L.; González, I. Ti Anodization in Alkaline Electrolyte: The Relationship between Transport of Defects, Film Hydration and Composition. *J. Electrochem. Soc.* **2013**, *160*, C277−C284.

(26) Pourbaix, M. In *Atlas of Electrochemical Equilibria in Aqueous Solutions*; National Association of Corrosion Engineers: Houston, TX, 1974.

(27) Schweitzer, P. A. In *Fundamentals of Corrosion: Mechanisms, Causes, and Preventative Methods*; Taylor and Francis: Boca Raton, FL, USA, 2010.

(28) Gerischer, H. On the Stability of Semiconductor Electrodes Against Photodecomposition. *J. Electroanal. Chem. Interfacial Electrochem.* **1977**, *82*, 133−143.

(29) Park, S.; Barber, M. E. Thermodynamic Stabilities of Semiconductor Electrodes. *J. Electroanal. Chem. Interfacial Electrochem.* **1979**, *99*, 67−75.

(30) Fujishima, A.; Inoue, T.; Watanabe, T.; Honda, K. Stabilization of Photoanodes in Electrochemical Photocells for Solar Energy Conversion. *Chem. Lett.* **1978**, *7*, 357−360.

(31) Chen, S.; Wang, L. Thermodynamic Oxidation and Reduction Potentials of Photocatalytic Semiconductors in Aqueous Solution. *Chem. Mater.* **2012**, *24*, 3659−3666.

(32) Nikolaychuk, P. The Revised Pourbaix Diagram for Silicon. *Silicon* **2014**, *6*, 109−116.

(33) Allongue, P.; Costa-Kieling, V.; Gerischer, H. Etching of Silicon in NaOH Solutions: I. in Situ Scanning Tunneling Microscopic Investigation of N-Si(111). *J. Electrochem. Soc.* **1993**, *140*, 1009−1018.

(34) Glembocki, O. J.; Stahlbush, R. E.; Tomkiewicz, M. Bias-Dependent Etching of Silicon in Aqueous KOH. *J. Electrochem. Soc.* **1985**, *132*, 145−151.

(35) Gronet, C. M.; Lewis, N. S. Design of a 13% Efficient n-$GaAs_{1-x}P_x$ Semiconductor-Liquid Junction Solar Cell. *Nature* **1982**, *300*, 733−735.

(36) Gronet, C. M.; Lewis, N. S.; Cogan, G.; Gibbons, J. N-Type Silicon Photoelectrochemistry in Methanol: Design of a 10.1% Efficient Semiconductor/Liquid Junction Solar Cell. *Proc. Natl. Acad. Sci. U. S. A.* **1983**, *80*, 1152−1156.

(37) Gratzel, M. Photoelectrochemical Cells. *Nature* **2001**, *414*, 338−344.

(38) Chang, K. C.; Heller, A.; Schwartz, B.; Menezes, S.; Miller, B. Stable Semiconductor Liquid Junction Cell with 9% Solar-to-Electrical Conversion Efficiency. *Science* **1977**, *196*, 1097−1099.

(39) Miller, B.; Heller, A. Semiconductor Liquid Junction Solar Cells Based on Anodic Sulphide Films. *Nature* **1976**, *262*, 680−681.

(40) Ellis, A. B.; Kaiser, S. W.; Wrighton, M. S. Visible Light to Electrical Energy Conversion. Stable Cadmium Sulfide and Cadmium Selenide Photoelectrodes in Aqueous Electrolytes. *J. Am. Chem. Soc.* **1976**, *98*, 1635−1637.

(41) Hodes, G.; Manassen, J.; Cahen, D. Photoelectrochemical Energy-Conversion and Storage using Polycrystalline Chalcogenide Electrodes. *Nature* **1976**, *261*, 403−404.

(42) Tufts, B. J.; Abrahams, I. L.; Casagrande, L. G.; Lewis, N. S. Studies of the Gallium Arsenide/Potassium Hydroxide-Selenium Ion (Se_2^{2-})/Selenide Semiconductor/Liquid Junction. *J. Phys. Chem.* **1989**, *93*, 3260−3269.

DOI: 10.1021/acs.jpcc.5b05976
J. Phys. Chem. C XXXX, XXX, XXX−XXX

(43) Seabold, J. A.; Choi, K. Efficient and Stable Photo-Oxidation of Water by a Bismuth Vanadate Photoanode Coupled with an Iron Oxyhydroxide Oxygen Evolution Catalyst. *J. Am. Chem. Soc.* **2012**, *134*, 2186−2192.
(44) Lichterman, M. F.; Shaner, M. R.; Handler, S. G.; Brunschwig, B. S.; Gray, H. B.; Lewis, N. S.; Spurgeon, J. M. Enhanced Stability and Activity for Water Oxidation in Alkaline Media with Bismuth Vanadate Photoelectrodes Modified with a Cobalt Oxide Catalytic Layer Produced by Atomic Layer Deposition. *J. Phys. Chem. Lett.* **2013**, *4*, 4188−4191.
(45) Bansal, A.; Lewis, N. S. Stabilization of Si Photoanodes in Aqueous Electrolytes through Surface Alkylation. *J. Phys. Chem. B* **1998**, *102*, 4058−4060.
(46) Bansal, A.; Li, X.; Lauermann, I.; Lewis, N. S.; Yi, S. I.; Weinberg, W. H. Alkylation of Si Surfaces using a Two-Step Halogenation/Grignard Route. *J. Am. Chem. Soc.* **1996**, *118*, 7225−7226.
(47) Bookbinder, D. C.; Bruce, J. A.; Dominey, R. N.; Lewis, N. S.; Wrighton, M. S. Synthesis and Characterization of a Photosensitive Interface for Hydrogen Generation: Chemically Modified P-Type Semiconducting Silicon Photocathodes. *Proc. Natl. Acad. Sci. U. S. A.* **1980**, *77*, 6280−6284.
(48) Campet, G.; Puprichitkun, C.; Sun, Z. W. Protection of Photoanodes Against Photocorrosion by Surface Deposition of Oxide Films: Criteria for Choosing the Protective Coating. *J. Electroanal. Chem. Interfacial Electrochem.* **1989**, *269*, 435−445.
(49) Hu, S.; Shaner, M. R.; Beardslee, J. A.; Lichterman, M.; Brunschwig, B. S.; Lewis, N. S. Amorphous TiO_2 Coatings Stabilize Si, GaAs, and GaP Photoanodes for Efficient Water Oxidation. *Science* **2014**, *344*, 1005−1009.
(50) Xiang, C.; Meng, A. C.; Lewis, N. S. Evaluation and Optimization of Mass Transport of Redox Species in Silicon Microwire-Array Photoelectrodes. *Proc. Natl. Acad. Sci. U. S. A.* **2012**, *109*, 15622−15627.
(51) Warren, E. L.; McKone, J. R.; Atwater, H. A.; Gray, H. B.; Lewis, N. S. Hydrogen-Evolution Characteristics of Ni-Mo-Coated, Radial Junction, n^+p-Silicon Microwire Array Photocathodes. *Energy Environ. Sci.* **2012**, *5*, 9653−9661.
(52) Roske, C. W.; Popczun, E. J.; Seger, B.; Read, C. G.; Pedersen, T.; Hansen, O.; Vesborg, P. C. K.; Brunschwig, B. S.; Schaak, R. E.; Chorkendorff, I.; Gray, H. B.; Lewis, N. S. Comparison of the Performance of CoP-Coated and Pt-Coated Radial Junctionn+p-Silicon Microwire-Array Photocathodes for the Sunlight-Driven Reduction of Water to H_2(g). *J. Phys. Chem. Lett.* **2015**, *6*, 1679−1683.
(53) Tsai, M.; Fahrenbruch, A. L.; Bube, R. H. Sputtered Oxide/Indium Phosphide Junctions and Indium Phosphide Surfaces. *J. Appl. Phys.* **1980**, *51*, 2696−2705.
(54) George, S. M. Atomic Layer Deposition: An Overview. *Chem. Rev.* **2010**, *110*, 111−131.
(55) Djokic, S. S., Ed. In *Electrodeposition: Theory and Practice*; Modern Aspects of Electrochemistry; Springer: New York, 2010.
(56) Kanan, M. W.; Surendranath, Y.; Nocera, D. G. Cobalt-Phosphate Oxygen-Evolving Compound. *Chem. Soc. Rev.* **2009**, *38*, 109−114.
(57) Lev, O.; Wu, Z.; Bharathi, S.; Glezer, V.; Modestov, A.; Gun, J.; Rabinovich, L.; Sampath, S. Solâ'Gel Materials in Electrochemistry. *Chem. Mater.* **1997**, *9*, 2354−2375.
(58) Yuan, J.; Tsujikawa, S. Characterization of Sol-Gel-Derived TiO2 Coatings and their Photoeffects on Copper Substrates. *J. Electrochem. Soc.* **1995**, *142*, 3444−3450.
(59) Warren, E. L.; Boettcher, S. W.; Walter, M. G.; Atwater, H. A.; Lewis, N. S. pH-Independent, 520 mV Open-Circuit Voltages of Si/Methyl Viologen$^{2+/+}$ Contacts through use of Radial n^+p-Si Junction Microwire Array Photoelectrodes. *J. Phys. Chem. C* **2011**, *115*, 594−598.
(60) Boettcher, S. W.; Spurgeon, J. M.; Putnam, M. C.; Warren, E. L.; Turner-Evans, D. B.; Kelzenberg, M. D.; Maiolo, J. R.; Atwater, H. A.; Lewis, N. S. Energy-Conversion Properties of Vapor-Liquid-Solid−Grown Silicon Wire-Array Photocathodes. *Science* **2010**, *327*, 185−187.
(61) Lin, F.; Boettcher, S. W. Adaptive Semiconductor/Electrocatalyst Junctions in Water-Splitting Photoanodes. *Nat. Mater.* **2014**, *13*, 81−86.
(62) Mills, T. J.; Lin, F.; Boettcher, S. W. Theory and Simulations of Electrocatalyst-Coated Semiconductor Electrodes for Solar Water Splitting. *Phys. Rev. Lett.* **2014**, *112*, 148304.
(63) Green, M. A.; Emery, K.; Hishikawa, Y.; Warta, W.; Dunlop, E. D. Solar Cell Efficiency Tables (Version 45). *Prog. Photovoltaics* **2015**, *23*, 1−9.
(64) Anderson, W. A.; Delahoy, A. E.; Milano, R. A. An 8% Efficient Layered Schottky-barrier Solar Cell. *J. Appl. Phys.* **1974**, *45*, 3913−3915.
(65) Manifacier, J. C.; Szepessy, L. Efficient Sprayed In_2O_3: Sn n-type Silicon Heterojunction Solar Cell. *Appl. Phys. Lett.* **1977**, *31*, 459−462.
(66) Godfrey, R. B.; Green, M. A. 655 mV Open-circuit Voltage, 17.6% Efficient Silicon MIS Solar Cells. *Appl. Phys. Lett.* **1979**, *34*, 790−793.
(67) Inzelt, G.; Lewenstam, A.; Scholz, F., Eds.; In *Handbook of Reference Electrodes*; Springer: New York, 2013.
(68) Strandwitz, N. C.; Comstock, D. J.; Grimm, R. L.; Nichols-Nielander, A. C.; Elam, J.; Lewis, N. S. Photoelectrochemical Behavior of N-Type Si(100) Electrodes Coated with Thin Films of Manganese Oxide Grown by Atomic Layer Deposition. *J. Phys. Chem. C* **2013**, *117*, 4931−4936.
(69) Sze, S. M.; Ng, K. K. In *Physics of Semiconductor Devices*, 3rd ed.; Wiley: New York, 2006; p 832.
(70) Nakato, Y.; Ohnishi, T.; Tsubomura, H. Photo-Electrochemical Behaviors of Semiconductor Electrodes Coated with Thin Metal Films. *Chem. Lett.* **1975**, 883−886.
(71) Harris, L. A.; Gerstner, M. E.; Wilson, R. H. The Role of Metal Overlayers on Gallium Phosphide Photoelectrodes. *J. Electrochem. Soc.* **1977**, *124*, 1511−1516.
(72) Kenney, M. J.; Gong, M.; Li, Y.; Wu, J. Z.; Feng, J.; Lanza, M.; Dai, H. High-Performance Silicon Photoanodes Passivated with Ultrathin Nickel Films for Water Oxidation. *Science* **2013**, *342*, 836−840.
(73) Mei, B.; Seger, B.; Pedersen, T.; Malizia, M.; Hansen, O.; Chorkendorff, I.; Vesborg, P. C. K. Protection of P+-N-Si Photoanodes by Sputter-Deposited Ir/IrO_x Thin Films. *J. Phys. Chem. Lett.* **2014**, *5*, 1948−1952.
(74) Conway, B. E.; Mozota, J. Surface and Bulk Processes at Oxidized Iridium electrodes—II. Conductivity-Switched Behaviour of Thick Oxide Films. *Electrochim. Acta* **1983**, *28*, 9−16.
(75) Yamane, S.; Kato, N.; Kojima, S.; Imanishi, A.; Ogawa, S.; Yoshida, N.; Nonomura, S.; Nakato, Y. Efficient Solar Water Splitting with a Composite ″n-Si/P-CuI/N-i-P a-Si/N-P GaP/RuO_2″ Semiconductor Electrode. *J. Phys. Chem. C* **2009**, *113*, 14575−14581.
(76) Hodes, G.; Thompson, L.; DuBow, J.; Rajeshwar, K. Heterojunction Silicon/Indium Tin Oxide Photoelectrodes: Development of Stable Systems in Aqueous Electrolytes and their Applicability to Solar Energy Conversion and Storage. *J. Am. Chem. Soc.* **1983**, *105*, 324−330.
(77) Reece, S. Y.; Hamel, J. A.; Sung, K.; Jarvi, T. D.; Esswein, A. J.; Pijpers, J. J. H.; Nocera, D. G. Wireless Solar Water Splitting using Silicon-Based Semiconductors and Earth-Abundant Catalysts. *Science* **2011**, *334*, 645−648.
(78) Rocheleau, R. E.; Miller, E. L.; Misra, A. High-Efficiency Photoelectrochemical Hydrogen Production using Multijunction Amorphous Silicon Photoelectrodes. *Energy Fuels* **1998**, *12*, 3−10.
(79) Kraft, A.; Görig, B.; Heckner, K. ITO Coated n-GaAs Electrodes for Photoelectrochemical Solar Cells. *Sol. Energy Mater. Sol. Cells* **1994**, *32*, 151−158.
(80) Sun, K.; Shen, S.; Cheung, J. S.; Pang, X.; Park, N.; Zhou, J.; Hu, Y.; Sun, Z.; Noh, S. Y.; Riley, C. T.; et al. Si Photoanode Protected by a Metal Modified ITO Layer with Ultrathin NiOx for Solar Water Oxidation. *Phys. Chem. Chem. Phys.* **2014**, *16*, 4612−4625.

DOI: 10.1021/acs.jpcc.5b05976
J. Phys. Chem. C XXXX, XXX, XXX−XXX

(81) Poznyak, S. K.; Makuta, I. D.; Kulak, A. I. Photoelectrochemical Behaviour of N-Silicon Photoanodes Coated with Chromium(III) Oxide Films and Cr_2O_3 Containing Composite Layers. *Sol. Energy Mater.* **1989**, *18*, 357−364.
(82) Contractor, A. Q.; Bockris, J. O. Investigation of a Protective Conducting Silica Film on N-Silicon. *Electrochim. Acta* **1984**, *29*, 1427−1434.
(83) Morisaki, H.; Ono, H.; Dohkoshi, H.; Yazawa, K. Iron-Oxide Coated N-Si as a Heterostructure Photoanode for the Photoelectrolysis of Water. *Jpn. J. Appl. Phys.* **1980**, *19*, L148.
(84) Nogami, G.; Yamaguchi, H.; Maeda, G.; Beppu, K.; Ueda, Y.; Nakamura, T. XPS and AES Studies on Iron-oxide-coated Si Photoanodes with a Negative Flatband Potential. *J. Appl. Phys.* **1983**, *54*, 1605−1609.
(85) Osaka, T.; Hirota, N.; Hayashi, T.; Eskildsen, S. S. Characteristics of Photoelectrochemical Cells with Iron Oxide/N-Si Heterojunction Photoanodes. *Electrochim. Acta* **1985**, *30*, 1209−1212.
(86) Osaka, T.; Ejiri, K.; Hirota, N. Photoelectrochemical Behavior of Iron Oxide/N-Si Heterojunction Electrodes with an Outer Pd Layer. *J. Electrochem. Soc.* **1984**, *131*, 1571−1574.
(87) Ono, H.; Morisaki, H.; Yazawa, K. Photoelectrochemical Properties of Iron-Oxide Films and the Coating Effects Onto n-Si as an Efficient Photoanode. *Jpn. J. Appl. Phys.* **1982**, *21*, 1075.
(88) Jun, K.; Lee, Y. S.; Buonassisi, T.; Jacobson, J. M. High Photocurrent in Silicon Photoanodes Catalyzed by Iron Oxide Thin Films for Water Oxidation. *Angew. Chem., Int. Ed.* **2012**, *51*, 423−427.
(89) Osaka, T.; Kitayama, H.; Hirota, N.; Eskildsen, S. S. Structural Analysis of Iron Oxide Coated N-Silicon Heterojunction Photoanodes. *Electrochim. Acta* **1984**, *29*, 1365−1370.
(90) Kainthla, R. C.; Zelenay, B.; Bockris, J. O. Protection of N-Si Photoanode Against Photocorrosion in Photoelectrochemical Cell for Water Electrolysis. *J. Electrochem. Soc.* **1986**, *133*, 248−253.
(91) Kainthla, R. C.; Zelenay, B.; Bockris, J. O. Significant Efficiency Increase in Self-Driven Photoelectrochemical Cell for Water Photoelectrolysis. *J. Electrochem. Soc.* **1987**, *134*, 841−845.
(92) Sun, K.; Park, N.; Sun, Z.; Zhou, J.; Wang, J.; Pang, X.; Shen, S.; Noh, S. Y.; Jing, Y.; Jin, S.; et al. Nickel Oxide Functionalized Silicon for Efficient Photo-Oxidation of Water. *Energy Environ. Sci.* **2012**, *5*, 7872−7877.
(93) Sun, K.; Pang, X.; Shen, S.; Qian, X.; Cheung, J. S.; Wang, D. Metal Oxide Composite Enabled Nanotextured Si Photoanode for Efficient Solar Driven Water Oxidation. *Nano Lett.* **2013**, *13*, 2064−2072.
(94) Yang, J.; Walczak, K.; Anzenberg, E.; Toma, F. M.; Yuan, G.; Beeman, J.; Schwartzberg, A.; Lin, Y.; Hettick, M.; Javey, A.; et al. Efficient and Sustained Photoelectrochemical Water Oxidation by Cobalt Oxide/Silicon Photoanodes with Nanotextured Interfaces. *J. Am. Chem. Soc.* **2014**, *136*, 6191−6194.
(95) Mei, B.; Permyakova, A. A.; Frydendal, R.; Bae, D.; Pedersen, T.; Malacrida, P.; Hansen, O.; Stephens, I. E. L.; Vesborg, P. C. K.; Seger, B.; et al. Iron-Treated NiO as a Highly Transparent P-Type Protection Layer for Efficient Si-Based Photoanodes. *J. Phys. Chem. Lett.* **2014**, *5*, 3456−3461.
(96) Sun, K.; McDowell, M. T.; Nielander, A. C.; Hu, S.; Shaner, M. R.; Yang, F.; Brunschwig, B. S.; Lewis, N. S. Stable Solar-Driven Water Oxidation to O_2(g) by Ni-Oxide-Coated Silicon Photoanodes. *J. Phys. Chem. Lett.* **2015**, *6*, 592−598.
(97) Sun, K.; Saadi, F. H.; Lichterman, M. F.; Hale, W. G.; Wang, H.; Zhou, X.; Plymale, N. T.; Omelchenko, S. T.; He, J.; Papadantonakis, K. M.; et al. Stable Solar-Driven Oxidation of Water by Semiconducting Photoanodes Protected by Transparent Catalytic Nickel Oxide Films. *Proc. Natl. Acad. Sci. U. S. A.* **2015**, *112*, 3612−3617.
(98) Chen, L.; Yang, J.; Klaus, S.; Lee, L. J.; Woods-Robinson, R.; Ma, J.; Lum, Y.; Cooper, J. K.; Toma, F. M.; Wang, L.; et al. P-Type Transparent Conducting Oxide/N-Type Semiconductor Heterojunctions for Efficient and Stable Solar Water Oxidation. *J. Am. Chem. Soc.* **2015**, *137*, 9595−9603.
(99) Abe, R.; Higashi, M.; Domen, K. Facile Fabrication of an Efficient Oxynitride TaON Photoanode for overall Water Splitting into H_2 and O_2 Under Visible Light Irradiation. *J. Am. Chem. Soc.* **2010**, *132*, 11828−11829.
(100) Higashi, M.; Domen, K.; Abe, R. Highly Stable Water Splitting on Oxynitride TaON Photoanode System Under Visible Light Irradiation. *J. Am. Chem. Soc.* **2012**, *134*, 6968−6971.
(101) Kim, E. S.; Nishimura, N.; Magesh, G.; Kim, J. Y.; Jang, J.; Jun, H.; Kubota, J.; Domen, K.; Lee, J. S. Fabrication of $CaFe_2O_4$/TaON Heterojunction Photoanode for Photoelectrochemical Water Oxidation. *J. Am. Chem. Soc.* **2013**, *135*, 5375−5383.
(102) Kim, E. S.; Kang, H. J.; Magesh, G.; Kim, J. Y.; Jang, J.; Lee, J. S. Improved Photoelectrochemical Activity of $CaFe_2O_4$/$BiVO_4$ Heterojunction Photoanode by Reduced Surface Recombination in Solar Water Oxidation. *ACS Appl. Mater. Interfaces* **2014**, *6*, 17762−17769.
(103) Liu, G.; Shi, J.; Zhang, F.; Chen, Z.; Han, J.; Ding, C.; Chen, S.; Wang, Z.; Han, H.; Li, C. A Tantalum Nitride Photoanode Modified with a Hole-Storage Layer for Highly Stable Solar Water Splitting. *Angew. Chem., Int. Ed.* **2014**, *53*, 7295−7299.
(104) Higashi, M.; Domen, K.; Abe, R. Fabrication of an Efficient $BaTaO_2N$ Photoanode Harvesting a Wide Range of Visible Light for Water Splitting. *J. Am. Chem. Soc.* **2013**, *135*, 10238−10241.
(105) Li, Y.; Zhang, L.; Torres-Pardo, A.; Gonzalez-Calbet, J. M.; Ma, Y.; Oleynikov, P.; Terasaki, O.; Asahina, S.; Shima, M.; Cha, D. Cobalt Phosphate-Modified Barium-Doped Tantalum Nitride Nanorod Photoanode with 1.5% Solar Energy Conversion Efficiency. *Nat. Commun.* **2013**, DOI: 10.1038/ncomms3566.
(106) Liao, M.; Feng, J.; Luo, W.; Wang, Z.; Zhang, J.; Li, Z.; Yu, T.; Zou, Z. Co3O4 Nanoparticles as Robust Water Oxidation Catalysts Towards Remarkably Enhanced Photostability of a Ta3N5 Photoanode. *Adv. Funct. Mater.* **2012**, *22*, 3066−3074.
(107) Ohara, W.; Uchida, D.; Hayashi, T.; Deura, M.; Ohkawa, K. Hydrogen Generation for 500 h by Photoelectrolysis of Water using GaN. *MRS Online Proc. Libr.* **2012**, DOI: 10.1557/opl.2012.1249.
(108) Hayashi, T.; Deura, M.; Ohkawa, K. High Stability and Efficiency of GaN Photocatalyst for Hydrogen Generation from Water. *Jpn. J. Appl. Phys.* **2012**, *51*, 112601.
(109) McDowell, M. T.; Lichterman, M. F.; Spurgeon, J. M.; Hu, S.; Sharp, I. D.; Brunschwig, B. S.; Lewis, N. S. Improved Stability of Polycrystalline Bismuth Vanadate Photoanodes by use of Dual-Layer Thin TiO2/Ni Coatings. *J. Phys. Chem. C* **2014**, *118*, 19618−19624.
(110) Zhong, D. K.; Choi, S.; Gamelin, D. R. Near-Complete Suppression of Surface Recombination in Solar Photoelectrolysis by "Co-Pi" Catalyst-Modified W:BiVO4. *J. Am. Chem. Soc.* **2011**, *133*, 18370−18377.
(111) McDonald, K. J.; Choi, K. A New Electrochemical Synthesis Route for a BiOI Electrode and its Conversion to a Highly Efficient Porous $BiVO_4$ Photoanode for Solar Water Oxidation. *Energy Environ. Sci.* **2012**, *5*, 8553−8557.
(112) Kim, T. W.; Choi, K. Nanoporous BiVO4 Photoanodes with Dual-Layer Oxygen Evolution Catalysts for Solar Water Splitting. *Science* **2014**, *343*, 990−994.
(113) Zhong, M.; et al. Surface Modification of CoOx Loaded $BiVO_4$ Photoanodes with Ultrathin P-Type NiO Layers for Improved Solar Water Oxidation. *J. Am. Chem. Soc.* **2015**, *137*, 5053.
(114) Kalanyan, B.; Parsons, G. Atomic Layer Deposited Oxides for Passivation of Silicon Photoelectrodes for Solar Photoelectrochemical Cells. *ECS Trans.* **2011**, *41*, 285−292.
(115) Robertson, J. Band Offsets of High Dielectric Constant Gate Oxides on Silicon. *J. Non-Cryst. Solids* **2002**, *303*, 94−100.
(116) Guo, L.; Hung, D.; Wang, W.; Shen, W.; Zhu, L.; Chien, C.; Searson, P. C. Tunnel Barrier Photoelectrodes for Solar Water Splitting. *Appl. Phys. Lett.* **2010**, *97*, 063111.
(117) Nishimura, N.; Raphael, B.; Maeda, K.; Le Gendre, L.; Abe, R.; Kubota, J.; Domen, K. Effect of $TiCl_4$ Treatment on the Photoelectrochemical Properties of $LaTiO_2N$ Electrodes for Water Splitting Under Visible Light. *Thin Solid Films* **2010**, *518*, 5855−5859.
(118) Higashi, M.; Domen, K.; Abe, R. Fabrication of Efficient TaON and Ta_3N_5 Photoanodes for Water Splitting Under Visible Light Irradiation. *Energy Environ. Sci.* **2011**, *4*, 4138−4147.

DOI: 10.1021/acs.jpcc.5b05976
J. Phys. Chem. C XXXX, XXX, XXX−XXX

(119) Chen, Y. W.; Prange, J. D.; Duhnen, S.; Park, Y.; Gunji, M.; Chidsey, C. E. D.; McIntyre, P. C. Atomic Layer-Deposited Tunnel Oxide Stabilizes Silicon Photoanodes for Water Oxidation. *Nat. Mater.* **2011**, *10*, 539−544.
(120) Scheuermann, A. G.; Prange, J. D.; Gunji, M.; Chidsey, C. E. D.; McIntyre, P. C. Effects of Catalyst Material and Atomic Layer Deposited TiO2 Oxide Thickness on the Water Oxidation Performance of Metal-Insulator-Silicon Anodes. *Energy Environ. Sci.* **2013**, *6*, 2487−2496.
(121) Liu, M.; Nam, C.; Black, C. T.; Kamcev, J.; Zhang, L. Enhancing Water Splitting Activity and Chemical Stability of Zinc Oxide Nanowire Photoanodes with Ultrathin Titania Shells. *J. Phys. Chem. C* **2013**, *117*, 13396−13402.
(122) Shaner, M. R.; Hu, S.; Sun, K.; Lewis, N. S. Stabilization of Si Microwire Arrays for Solar-Driven H_2O Oxidation to O_2(g) in 1.0 M KOH(Aq) using Conformal Coatings of Amorphous TiO_2. *Energy Environ. Sci.* **2015**, *8*, 203−207.
(123) Mei, B.; Pedersen, T.; Malacrida, P.; Bae, D.; Frydendal, R.; Hansen, O.; Vesborg, P. C. K.; Seger, B.; Chorkendorff, I. Crystalline TiO_2: A Generic and Effective Electron-Conducting Protection Layer for Photoanodes and -Cathodes. *J. Phys. Chem. C* **2015**, *119*, 15019−15027.
(124) Tu, D.; Wang, H.; Wang, P.; Cheng, W.; Chen, K.; Wu, C.; Chattopadhyay, S.; Chen, L. Improved Corrosion Resistance of GaN Electrodes in NaCl Electrolyte for Photoelectrochemical Hydrogen Generation. *Int. J. Hydrogen Energy* **2013**, *38*, 14433−14439.
(125) Fujii, K.; Kato, T.; Sato, K.; Im, I.; Chang, J.; Yao, T. Photoelectrochemical Application of GaN Nanostructures on Si for Hydrogen Generation by Water Reduction. *Phys. Status Solidi C* **2010**, *7*, 2218−2220.
(126) Ginley, D. S.; Baughman, R. J.; Butler, M. A. BP-Stabilized n-Si and n - GaAs Photoanodes. *J. Electrochem. Soc.* **1983**, *130*, 1999−2002.
(127) Goossens, A.; Kelder, E. M.; Beeren, R. J. M.; Bartels, C. J. G.; Schoonman, J. Structural, Optical, and Electronic Properties of Silicon/Boron Phosphide Heterojunction Photoelectrodes. *Berichte der Bunsengesellschaft für physikalische Chemie* **1991**, *95*, 503−510.
(128) Fan, F. R. F.; Keil, R. G.; Bard, A. J. Semiconductor Electrodes. 48. Photooxidation of Halides and Water on N-Silicon Protected with Silicide Layers. *J. Am. Chem. Soc.* **1983**, *105*, 220−224.
(129) Nakato, Y.; Hiramoto, M.; Iwakabe, Y.; Tsubomura, H. ESCA and Photoelectrochemical Studies of p-n Junction Silicon Electrodes Protected by Platinum Deposition for use in Solar Energy Conversion. *J. Electrochem. Soc.* **1985**, *132*, 330−334.
(130) Nakato, Y.; Tsubomura, H. Silicon Photoelectrodes Modified with Ultrafine Metal Islands. *Electrochim. Acta* **1992**, *37*, 897−907.
(131) Thompson, L.; DuBow, J.; Rajeshwar, K. Photoelectrochemical Generation of Chlorine on Catalytically Modified N-Silicon/Indium Tin Oxide Anodes. *J. Electrochem. Soc.* **1982**, *129*, 1934−1935.
(132) Decker, F.; Fracastoro-Decker, M.; Badawy, W.; Doblhofer, K.; Gerischer, H. The Photocurrent-Voltage Characteristics of the Heterojunction Combination n - Si/SnO_2/Redox - Electrolyte. *J. Electrochem. Soc.* **1983**, *130*, 2173−2179.
(133) Bélanger, D.; Dodelet, J. P.; Lombos, B. A. Characteristics and Stability of n - Si/SnO_2 and n - Si/SnO_2/Pt Photoanodes. *J. Electrochem. Soc.* **1986**, *133*, 1113−1119.
(134) Tsubomura, H.; Nakato, Y.; Hiramoto, M.; Yano, H. Metal Oxide Coated P-N Junction Silicon Electrodes for Photoelectrochemical Solar Energy Conversion. *Can. J. Chem.* **1985**, *63*, 1759−1762.
(135) Nakato, Y.; Tsumura, A.; Tsubomura, H. Efficient Photoelectrochemical Conversion of Solar Energy with N-Type Silicon Semiconductor Electrodes Surface-Doped with IIIA-Group Elements. *Chem. Lett.* **1982**, *11*, 1071−1074.
(136) Palik, E. D.; Faust, J. W.; Gray, H. F.; Greene, R. F. Study of the Etch-Stop Mechanism in Silicon. *J. Electrochem. Soc.* **1982**, *129*, 2051−2059.
(137) Simon, R. A.; Wrighton, M. S. Stabilization of N-type Silicon Photoanodes Against Photoanodic Decomposition with Thin Films of Polyacetylene. *Appl. Phys. Lett.* **1984**, *44*, 930−932.
(138) Mubeen, S.; Lee, J.; Singh, N.; Moskovits, M.; McFarland, E. W. Stabilizing Inorganic Photoelectrodes for Efficient Solar-to-Chemical Energy Conversion. *Energy Environ. Sci.* **2013**, *6*, 1633−1639.
(139) Takabayashi, S.; Nakamura, R.; Nakato, Y. A Nano-Modified Si/TiO2 Composite Electrode for Efficient Solar Water Splitting. *J. Photochem. Photobiol., A* **2004**, *166*, 107−113.
(140) Kohl, P. A.; Frank, S. N.; Bard, A. J. Semiconductor Electrodes XI. Behavior of N and P-Type Single Crystal Semconductors Covered with Thin TiO2 Films. *J. Electrochem. Soc.* **1977**, *124*, 225−229.
(141) Tomkiewicz, M.; Woodall, J. M. Photoelectrolysis of Water with Semiconductor Materials. *J. Electrochem. Soc.* **1977**, *124*, 1436−1440.
(142) Li, G.; Wang, S. Photoelectrochemical Characteristics of Metal-Modified Epitaxial N-Si Anodes: Part I. NiO(OH)-Coated N+/P-Si and N+/N-Si Electrodes for Catalytic Oxygen Evolution. *J. Electroanal. Chem. Interfacial Electrochem.* **1987**, *227*, 213−221.
(143) Miller, E. L.; Rocheleau, R. E.; Khan, S. A Hybrid Multijunction Photoelectrode for Hydrogen Production Fabricated with Amorphous Silicon/Germanium and Iron Oxide Thin Films. *Int. J. Hydrogen Energy* **2004**, *29*, 907−914.
(144) Lichterman, M. F.; Carim, A. I.; McDowell, M. T.; Hu, S.; Gray, H. B.; Brunschwig, B. S.; Lewis, N. S. Stabilization of N-Cadmium Telluride Photoanodes for Water Oxidation to O2(G) in Aqueous Alkaline Electrolytes using Amorphous TiO2 Films Formed by Atomic-Layer Deposition. *Energy Environ. Sci.* **2014**, *7*, 3334−3337.
(145) Li, C.; Wang, T.; Luo, Z.; Zhang, D.; Gong, J. Transparent ALD-Grown Ta2O5 Protective Layer for Highly Stable ZnO Photoelectrode in Solar Water Splitting. *Chem. Commun.* **2015**, *51*, 7290.
(146) Sun, K.; Kuang, Y.; Verlage, E.; Brunschwig, B. S.; Tu, C. W.; Lewis, N. S. Sputtered NiOx Films for Stabilization of P+n-InP Photoanodes for Solar-Driven Water Oxidation. *Adv. En. Mater.* **2015**, DOI: 10.1002/aenm.201570059.
(147) Leempoel, P.; Castro-Acuna, M.; Fan, F. F.; Bard, A. J. Semiconductor Electrodes. 43. the Effect of Light Intensity and Iodine Doping on the Stabilization of N-Silicon by Phthalocyanine Films. *J. Phys. Chem.* **1982**, *86*, 1396−1400.
(148) Heller, A. Hydrogen Evolving Solar Cells. *Catal. Rev.: Sci. Eng.* **1984**, *26*, 655−681.
(149) Peter, L. M.; Li, J.; Peat, R. Surface Recombination at Semiconductor Electrodes: Part I. Transient and Steady-State Photocurrents. *J. Electroanal. Chem. Interfacial Electrochem.* **1984**, *165*, 29−40.
(150) Heller, A.; Vadimsky, R. G. Efficient Solar to Chemical Conversion: 12% Efficient Photoassisted Electrolysis in the p-Type InP(Ru)]/HCl-KCl/Pt(Rh) Cell. *Phys. Rev. Lett.* **1981**, *46*, 1153−1156.
(151) Heller, A.; Aharon-Shalom, E.; Bonner, W. A.; Miller, B. Hydrogen-Evolving Semiconductor Photocathodes: Nature of the Junction and Function of the Platinum Group Metal Catalyst. *J. Am. Chem. Soc.* **1982**, *104*, 6942−6948.
(152) Sakai, Y.; Sugahara, S.; Matsumura, M.; Nakato, Y.; Tsubomura, H. Photoelectrochemical Water Splitting by Tandem Type and Heterojunction Amorphous Silicon Electrodes. *Can. J. Chem.* **1988**, *66*, 1853−1856.
(153) Maier, C. U.; Specht, M.; Bilger, G. Hydrogen Evolution on Platinum-Coated P-Silicon Photocathodes. *Int. J. Hydrogen Energy* **1996**, *21*, 859.
(154) Khaselev, O.; Turner, J. A. Photoelectrolysis of HBr and HI using a Monolithic Combined Photoelectrochemical/Photovoltaic Device. *Electrochem. Solid-State Lett.* **1999**, *2*, 310−312.
(155) Siripala, W.; Ivanovskaya, A.; Jaramillo, T. F.; Baeck, S.; McFarland, E. W. A Cu_2O/TiO_2 Heterojunction Thin Film Cathode for Photoelectrocatalysis. *Sol. Energy Mater. Sol. Cells* **2003**, *77*, 229.
(156) Marsen, B.; Cole, B.; Miller, E. L. Photoelectrolysis of Water using Thin Copper Gallium Diselenide Electrodes. *Sol. Energy Mater. Sol. Cells* **2008**, *92*, 1054.

DOI: 10.1021/acs.jpcc.5b05976
J. Phys. Chem. C XXXX, XXX, XXX−XXX

(157) Yokoyama, D.; Minegishi, T.; Maeda, K.; Katayama, M.; Kubota, J.; Yamada, A.; Konagai, M.; Domen, K. Photoelectrochemical Water Splitting using a Cu(in,Ga)Se_2 Thin Film. *Electrochem. Commun.* **2010**, *12*, 851.
(158) Hou, Y.; Abrams, B. L.; Vesborg, P. C. K.; Bjarketun, M. E.; Herbst, K.; Bech, L.; Setti, A. M.; Damsgaard, C. D.; Pedersen, T.; Hansen, O.; et al. Bioinspired Molecular Co-Catalysts Bonded to a Silicon Photocathode for Solar Hydrogen Evolution. *Nat. Mater.* **2011**, *10*, 434−438.
(159) Lin, C.; Lai, Y.; Mersch, D.; Reisner, E. $Cu_2O|NiO_x$ Nanocomposite as an Inexpensive Photocathode in Photoelectrochemical Water Splitting. *Chem. Sci.* **2012**, *3*, 3482−3487.
(160) Paracchino, A.; Laporte, V.; Sivula, K.; Grätzel, M.; Thimsen, E. Highly Active Oxide Photocathode for Photoelectrochemical Water Reduction. *Nat. Mater.* **2011**, *10*, 456.
(161) Lee, M. H.; Takei, K.; Zhang, J.; Kapadia, R.; Zheng, M.; Chen, Y.; Nah, J.; Matthews, T. S.; Chueh, Y.; Ager, J. W.; Javey, A. P-Type InP Nanopillar Photocathodes for Efficient Solar-Driven Hydrogen Production. *Angew. Chem., Int. Ed.* **2012**, *51*, 10760−10764.
(162) Seger, B.; Laursen, A. B.; Vesborg, P. C. K.; Pedersen, T.; Hansen, O.; Dahl, S.; Chorkendorff, I. Hydrogen Production using a Molybdenum Sulfide Catalyst on a Titanium-Protected N+p-Silicon Photocathode. *Angew. Chem., Int. Ed.* **2012**, *51*, 9128−9131.
(163) Sun, K.; Madsen, K.; Andersen, P.; Bao, W.; Sun, Z.; Wang, D. Metal on Metal Oxide Nanowire Co-Catalyzed Si Photocathode for Solar Water Splitting. *Nanotechnology* **2012**, *23*, 194013.
(164) Paracchino, A.; Mathews, N.; Hisatomi, T.; Stefik, M.; Tilley, S. D.; Gratzel, M. Ultrathin Films on Copper(i) Oxide Water Splitting Photocathodes: A Study on Performance and Stability. *Energy Environ. Sci.* **2012**, *5*, 8673−8681.
(165) Rovelli, L.; Tilley, S. D.; Sivula, K. Optimization and Stabilization of Electrodeposited Cu_2ZnSnS_4 Photocathodes for Solar Water Reduction. *ACS Appl. Mater. Interfaces* **2013**, *5*, 8018−8024.
(166) Laursen, A. B.; Pedersen, T.; Malacrida, P.; Seger, B.; Hansen, O.; Vesborg, P. C. K.; Chorkendorff, I. MoS_2-an Integrated Protective and Active Layer on n^+p-Si for Solar H_2 Evolution. *Phys. Chem. Chem. Phys.* **2013**, *15*, 20000−20004.
(167) Moriya, M.; Minegishi, T.; Kumagai, H.; Katayama, M.; Kubota, J.; Domen, K. Stable Hydrogen Evolution from CdS-Modified $CuGaSe_2$ Photoelectrode Under Visible-Light Irradiation. *J. Am. Chem. Soc.* **2013**, *135*, 3733−3735.
(168) Yang, F.; Kuznietsov, V.; Lublow, M.; Merschjann, C.; Steigert, A.; Klaer, J.; Thomas, A.; Schedel-Niedrig, T. Solar Hydrogen Evolution using Metal-Free Photocatalytic Polymeric Carbon Nitride/$CuInS_2$ Composites as Photocathodes. *J. Mater. Chem. A* **2013**, *1*, 6407−6415.
(169) Seger, B.; Pedersen, T.; Laursen, A. B.; Vesborg, P. C. K.; Hansen, O.; Chorkendorff, I. Using TiO_2 as a Conductive Protective Layer for Photocathodic H_2 Evolution. *J. Am. Chem. Soc.* **2013**, *135*, 1057−1064.
(170) Lin, Y.; Battaglia, C.; Boccard, M.; Hettick, M.; Yu, Z.; Ballif, C.; Ager, J. W.; Javey, A. Amorphous Si Thin Film Based Photocathodes with High Photovoltage for Efficient Hydrogen Production. *Nano Lett.* **2013**, *13*, 5615−5618.
(171) Zhang, Z.; Dua, R.; Zhang, L.; Zhu, H.; Zhang, H.; Wang, P. Carbon-Layer-Protected Cuprous Oxide Nanowire Arrays for Efficient Water Reduction. *ACS Nano* **2013**, *7*, 1709−1717.
(172) Bourgeteau, T.; Tondelier, D.; Geffroy, B.; Brisse, R.; Laberty-Robert, C.; Campidelli, S.; de Bettignies, R.; Artero, V.; Palacin, S.; Jousselme, B. A H2-Evolving Photocathode Based on Direct Sensitization of MoS_3 with an Organic Photovoltaic Cell. *Energy Environ. Sci.* **2013**, *6*, 2706−2713.
(173) Esposito, D. V.; Levin, I.; Moffat, T. P.; Talin, A. A. H_2 Evolution at Si-Based Metal-Insulator-Semiconductor Photoelectrodes Enhanced by Inversion Channel Charge Collection and H Spillover. *Nat. Mater.* **2013**, *12*, 562−568.
(174) Morales-Guio, C. G.; Tilley, S. D.; Vrubel, H.; Gratzel, M.; Hu, X. Hydrogen Evolution from a Copper(I) Oxide Photocathode Coated with an Amorphous Molybdenum Sulphide Catalyst. *Nat. Commun.* **2014**, *5*, 3059.
(175) Benck, J. D.; Lee, S. C.; Fong, K. D.; Kibsgaard, J.; Sinclair, R.; Jaramillo, T. F. Designing Active and Stable Silicon Photocathodes for Solar Hydrogen Production using Molybdenum Sulfide Nanomaterials. *Adv. En. Mater.* **2014**, *4*, 1400739.
(176) Tilley, S. D.; Schreier, M.; Azevedo, J.; Stefik, M.; Graetzel, M. Ruthenium Oxide Hydrogen Evolution Catalysis on Composite Cuprous Oxide Water-Splitting Photocathodes. *Adv. Funct. Mater.* **2014**, *24*, 303−311.
(177) Choi, M. J.; Jung, J.; Park, M.; Song, J.; Lee, J.; Bang, J. H. Long-Term Durable Silicon Photocathode Protected by a Thin Al_2O_3/SiO_x Layer for Photoelectrochemical Hydrogen Evolution. *J. Mater. Chem. A* **2014**, *2*, 2928−2933.
(178) Kast, M. G.; Enman, L. J.; Gurnon, N. J.; Nadarajah, A.; Boettcher, S. W. Solution-Deposited F:SnO_2/TiO_2 as a Base-Stable Protective Layer and Antireflective Coating for Microtextured Buried-Junction H_2-Evolving Si Photocathodes. *ACS Appl. Mater. Interfaces* **2014**, *6*, 22830−22837.
(179) Lin, Y.; Kapadia, R.; Yang, J.; Zheng, M.; Chen, K.; Hettick, M.; Yin, X.; Battaglia, C.; Sharp, I. D.; Ager, J. W.; Javey, A. Role of TiO_2 Surface Passivation on Improving the Performance of p-InP Photocathodes. *J. Phys. Chem. C* **2015**, *119*, 2308−2313.
(180) Feng, J.; Gong, M.; Kenney, M.; Wu, J.; Zhang, B.; Li, Y.; Dai, H. Nickel-Coated Silicon Photocathode for Water Splitting in Alkaline Electrolytes. *Nano Res.* **2015**, *8*, 1577−1583.
(181) Fan, R.; Dong, W.; Fang, L.; Zheng, F.; Su, X.; Zou, S.; Huang, J.; Wang, X.; Shen, M. Stable and Efficient Multi-Crystalline n^+p Silicon Photocathode for H_2 Production with Pyramid-Like Surface Nanostructure and Thin Al_2O_3 Protective Layer. *Appl. Phys. Lett.* **2015**, *106*, 013902.
(182) Ji, L.; McDaniel, M. D.; Wang, S.; Posadas, A. B.; Li, X.; Huang, H.; Lee, J. C.; Demkov, A. A.; Bard, A. J.; Ekerdt, J. G.; Yu, E. T. A Silicon-Based Photocathode for Water Reduction with an Epitaxial $SrTiO_3$ Protection Layer and a Nanostructured Catalyst. *Nat. Nanotechnol.* **2015**, *10*, 84−90.
(183) Dominey, R. N.; Lewis, N. S.; Bruce, J. A.; Bookbinder, D. C.; Wrighton, M. S. Improvement of Photoelectrochemical Hydrogen Generation by Surface Modification of p-Type Silicon Semiconductor Photocathodes. *J. Am. Chem. Soc.* **1982**, *104*, 467−482.
(184) Hodes, G.; J, F.; Heller, A.; Miller, B. Photoelectrochemical Cells Based on Polycrystalline Semiconductors. *J. Electrochem. Soc.* **1984**, *13*, 2252.
(185) Oh, J.; Deutsch, T. G.; Yuan, H.; Branz, H. M. Nanoporous Black Silicon Photocathode for H2 Production by Photoelectrochemical Water Splitting. *Energy Environ. Sci.* **2011**, *4*, 1690−1694.
(186) Oh, I.; Kye, J.; Hwang, S. Enhanced Photoelectrochemical Hydrogen Production from Silicon Nanowire Array Photocathode. *Nano Lett.* **2012**, *12*, 298−302.
(187) Dasgupta, N. P.; Liu, C.; Andrews, S.; Prinz, F. B.; Yang, P. Atomic Layer Deposition of Platinum Catalysts on Nanowire Surfaces for Photoelectrochemical Water Reduction. *J. Am. Chem. Soc.* **2013**, *135*, 12932−12935.
(188) Dai, P.; Xie, J.; Mayer, M. T.; Yang, X.; Zhan, J.; Wang, D. Solar Hydrogen Generation by Silicon Nanowires Modified with Platinum Nanoparticle Catalysts by Atomic Layer Deposition. *Angew. Chem.* **2013**, *125*, 11325−11329.
(189) McKone, J. R.; Sadtler, B. F.; Werlang, C. A.; Lewis, N. S.; Gray, H. B. Ni-Mo Nanopowders for Efficient Electrochemical Hydrogen Evolution. *ACS Catal.* **2013**, *3*, 166−169.
(190) Seger, B.; Tilley, D. S.; Pedersen, T.; Vesborg, P. C. K.; Hansen, O.; Gratzel, M.; Chorkendorff, I. Silicon Protected with Atomic Layer Deposited TiO2: Durability Studies of Photocathodic H_2 Evolution. *RSC Adv.* **2013**, *3*, 25902−25907.
(191) Prasittichai, C.; Avila, J. R.; Farha, O. K.; Hupp, J. T. Systematic Modulation of Quantum (Electron) Tunneling Behavior by Atomic Layer Deposition on Nanoparticulate SnO_2 and TiO_2 Photoanodes. *J. Am. Chem. Soc.* **2013**, *135*, 16328−16331.

DOI: 10.1021/acs.jpcc.5b05976
J. Phys. Chem. C XXXX, XXX, XXX−XXX

(192) Miller, E. L.; Rocheleau, R. E.; Deng, X. M. Design Considerations for a Hybrid Amorphous Silicon/Photoelectrochemical Multijunction Cell for Hydrogen Production. *Int. J. Hydrogen Energy* **2003**, *28*, 615.
(193) Toor, F.; Deutsch, T. G.; Pankow, J. W.; Nemeth, W.; Nozik, A. J.; Branz, H. M. Novel Micropixelation Strategy to Stabilize Semiconductor Photoelectrodes for Solar Water Splitting Systems. *J. Phys. Chem. C* **2012**, *116*, 19262−19267.
(194) Yamada, Y.; Matsuki, N.; Ohmori, T.; Mametsuka, H.; Kondo, M.; Matsuda, A.; Suzuki, E. One Chip Photovoltaic Water Electrolysis Device. *Int. J. Hydrogen Energy* **2003**, *28*, 1167−1169.
(195) Johnson, E. L. In *In The TI Solar Energy System Development*; Electron Devices Meeting, 1981 International; 1981; Vol. *27*, pp 2−5. 10.1109/IEDM.1981.189984
(196) McKee, W. Development of the Spherical Silicon Solar Cell. *IEEE Trans. Compon., Hybrids, Manuf. Technol.* **1982**, *5*, 336−341.
(197) Kilby, J. S.; Lathrop, J. W.; Porter, W. A. US Patent, *Light Energy Conversion*, US 05/747,031, US4136436 A, 1979.
(198) Luttmer, J. D.; Konrad, D.; Trachtenberg, I. Electrode Materials for Hydrobromic Acid Electrolysis in Texas Instruments' Solar Chemical Converter. *J. Electrochem. Soc.* **1985**, *132*, 1054−1058.
(199) Kaiser, B.; Fertig, D.; Ziegler, J.; Klett, J.; Hoch, S.; Jaegermann, W. Solar Hydrogen Generation with Wide-Band-Gap Semiconductors: GaP(100) Photoelectrodes and Surface Modification. *ChemPhysChem* **2012**, *13*, 3053−3060.
(200) Aharon-Shalom, E.; Heller, A. Efficient p-InP (Rh- H alloy) and p-InP (Re-H alloy) Hydrogen Evolving Photocathodes. *J. Electrochem. Soc.* **1982**, *129*, 2865−2866.
(201) Heller, A. Conversion of Sunlight into Electrical Power and Photoassisted Electrolysis of Water in Photoelectrochemical Cells. *Acc. Chem. Res.* **1981**, *14*, 154−162.
(202) Lewerenz, H. J.; Schulte, K. H. Combined Photoelectrochemical Conditioning and Surface Analysis of InP Photocathodes: II. Photoelectron Spectroscopy. *Electrochim. Acta* **2002**, *47*, 2639.
(203) Lewerenz, H. Epitaxial III-V Thin Film Absorbers: Preparation, Efficient InP Photocathodes and Routes to High Efficiency Tandem Structures. *Photoelectrochemical Water Splitting: Materials, Processes and Architectures* **2013**, *9*, 223.
(204) Khaselev, O.; Turner, J. A. A Monolithic Photovoltaic-Photoelectrochemical Device for Hydrogen Production Via Water Splitting. *Science* **1998**, *280*, 425−427.
(205) Wang, H.; Deutsch, T.; Welch, A.; Turner, J. A. The Stability of Illuminated P-$GaInP_2$ Semiconductor Photoelectrode. *Int. J. Hydrogen Energy* **2012**, *37*, 14009.
(206) Deutsch, T. G.; Head, J. L.; Turner, J. A. Photoelectrochemical Characterization and Durability Analysis of GaInPN Epilayers. *J. Electrochem. Soc.* **2008**, *155*, B903−B907.
(207) Deutsch, T. G.; Welch, A.; Bär, M.; Weinhardt, L.; Weir, M. G.; George, K. E.; Heske, C.; Turner, J. A. Photoelectrolysis on P-GaInP2; Extended Durability by Nitrogen Ion Implantation. *ECS Meeting Abstracts* 2012, *MA2012−02*, 1743.
(208) Kargar, A.; Jing, Y.; Kim, S. J.; Riley, C. T.; Pan, X.; Wang, D. ZnO/CuO Heterojunction Branched Nanowires for Photoelectrochemical Hydrogen Generation. *ACS Nano* **2013**, *7*, 11112−11120.
(209) Zhao, J.; Minegishi, T.; Zhang, L.; Zhong, M.; Gunawan; Nakabayashi, M.; Ma, G.; Hisatomi, T.; Katayama, M.; Ikeda, S.; et al. Enhancement of Solar Hydrogen Evolution from Water by Surface Modification with CdS and TiO_2 on Porous $CuInS_2$ Photocathodes Prepared by an Electrodeposition-Sulfurization Method. *Angew. Chem., Int. Ed.* **2014**, *53*, 11808−11812.
(210) Gunawan; Septina, W.; Ikeda, S.; Harada, T.; Minegishi, T.; Domen, K.; Matsumura, M. Platinum and Indium Sulfide-Modified $CuInS_2$ as Efficient Photocathodes for Photoelectrochemical Water Splitting. *Chem. Commun.* **2014**, *50*, 8941−8943.
(211) Jacobsson, T. J.; Platzer-Björkman, C.; Edoff, M.; Edvinsson, T. $CuIn_xGa_{1-X}Se_2$ as an Efficient Photocathode for Solar Hydrogen Generation. *Int. J. Hydrogen Energy* **2013**, *38*, 15027.
(212) Wang, X.; Maeda, K.; Chen, X.; Takanabe, K.; Domen, K.; Hou, Y.; Fu, X.; Antonietti, M. Polymer Semiconductors for Artificial Photosynthesis: Hydrogen Evolution by Mesoporous Graphitic Carbon Nitride with Visible Light. *J. Am. Chem. Soc.* **2009**, *131*, 1680−1681.
(213) Wurfel, U.; Cuevas, A.; Wurfel, P. Charge Carrier Separation in Solar Cells. *Photovoltaics, IEEE Journal of* **2015**, *5*, 461−469.
(214) De Wolf, S.; Descoeudres, A.; Holman, Z. C.; Ballif, C. High-Efficiency Silicon Heterojunction Solar Cells: A Review. *Green* **2012**, *2*, 7.
(215) Taguchi, M.; Yano, A.; Tohoda, S.; Matsuyama, K.; Nakamura, Y.; Nishiwaki, T.; Fujita, K.; Maruyama, E. 24.7% Record Efficiency HIT Solar Cell on Thin Silicon Wafer. *Photovoltaics, IEEE Journal of* **2014**, *4*, 96−99.
(216) Chen, Z.; Jaramillo, T. F.; Deutsch, T. G.; Kleiman-Shwarsctein, A.; Forman, A. J.; Gaillard, N.; Garland, R.; Takanabe, K.; Heske, C.; Sunkara, M.; et al. Accelerating Materials Development for Photoelectrochemical Hydrogen Production: Standards for Methods, Definitions, and Reporting Protocols. *J. Mater. Res.* **2010**, *25*, 3−16.
(217) Parkinson, B. On the Efficiency and Stability of Photoelectrochemical Devices. *Acc. Chem. Res.* **1984**, *17*, 431−437.
(218) Deutsch, T. G.; Koval, C. A.; Turner, J. A. III-V Nitride Epilayers for Photoelectrochemical Water Splitting: GaPN and GaAsPN. *J. Phys. Chem. B* **2006**, *110*, 25297−25307.
(219) U.S. Department of Energy Technical Plan: Hydrogen Production, Multi-Year Research, Development and Demonstration Plan: Planned Program Activities for 2005−2015. 2007.
(220) Turner-Evans, D. B.; Emmer, H.; Chen, C. T.; Atwater, H. A. Flexible, Transparent Contacts for Inorganic Nanostructures and Thin Films. *Adv. Mater.* **2013**, *25*, 4018−4022.
(221) Nielander, A. C.; Bierman, M. J.; Petrone, N.; Strandwitz, N. C.; Ardo, S.; Yang, F.; Hone, J.; Lewis, N. S. Photoelectrochemical Behavior of N-Type Si(111) Electrodes Coated with a Single Layer of Graphene. *J. Am. Chem. Soc.* **2013**, *135*, 17246−17249.

DOI: 10.1021/acs.jpcc.5b05976
J. Phys. Chem. C XXXX, XXX, XXX−XXX